Getting to know small and big (soft matter) systems with scanning probe microscopy

José L. Toca-Herrera

Institute for Biophysics
Department of Nanobiotechnology (DNBT)
BOKU- University of Natural Resources and Life Sciences
Muthgasse 11, A-1190 Vienna, AUSTRIA

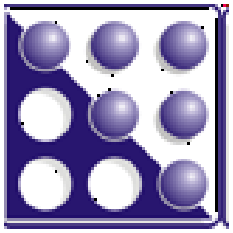

AGH, Krakow – 10/04/2015

Universität für Bodenkultur - BOKU

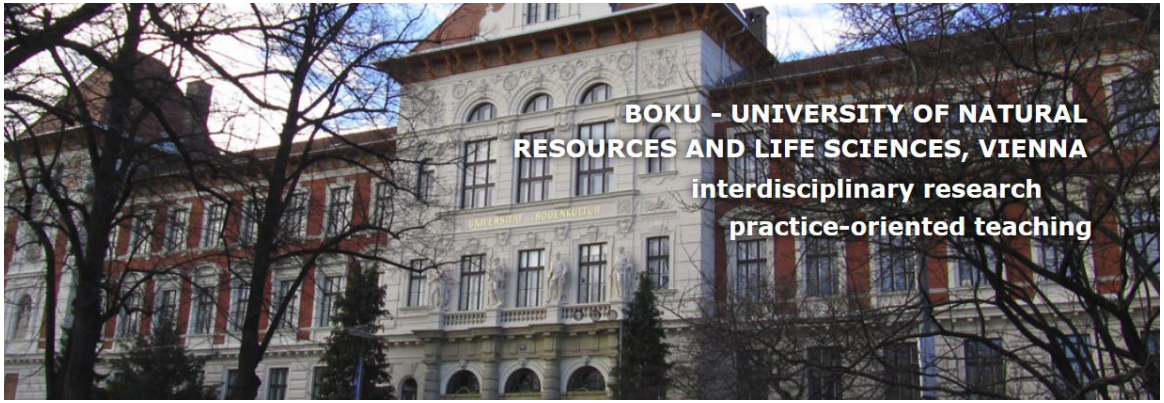

- Founded in 1872.

- First offered study programs: Agricultural-, Forestry studies, Environmental Engineering, Food Science and Biotechnology, and Landscape Planning and Environmental Studies.

- Today BOKU offers 9 Bachelor and 25 Master programs for more than 12.000 students (with about 2000 non-Austrians).

- Figures: 2600 workers, about 2000 students finished their degress, 2166 publications (685 SCI), 41.7 Millionen Euro (Projects).

Where are we (DNBT)?

Who are we - organisation?

Dept. Nanobiotechnology

Bioarchitectures	**Supr. Insp. Materials**	**Biophysics**
Eva Sinner	Erik Reimhult	Jose. L. Toca-Herrera

Full Professors / Chairs: 3
Emeritus Professor: 1
Associate Professors: 4
Univ. Assist. /postdocs: 13
Administration: 1 (+ 0.5)

PhD students: 20
MSc students: 17
BSc students: 5
Technical assistants: 6

We are also hosting PhD and MSc students of other universities or institutes!

DNBT – Research Eva Sinner

Nanobiotechnology I

- **Synthetic biology** is the engineering of biology: the synthesis of complex, biologically based (or inspired) systems which display functions that do not exist in nature

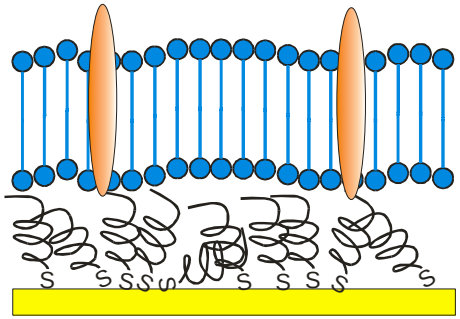

- Peptide P19
- CHO membrane (with *hPepT1*)

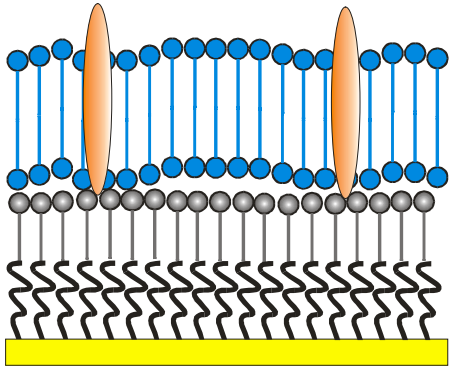

- Octadecanthiol
- Lipid
- CHO membrane (with *hPepT1*)

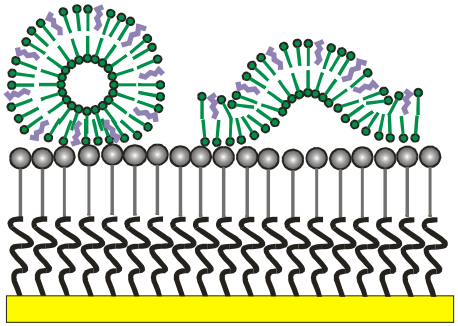

- Octadecanthiol
- Lipid
- PC/Cholesterol vesicles

DNBT – Research Erik Reimhult

Nanobiotechnology II

- **Supramolecular (bio)materials** - nanoscale building blocks enables controlled interfacial assembly
- (Bioinspired) liquid-liquid interfaces allow energy mimization by attaining ordering of adsorbed nanoparticles
- Dispersed nanoparticles can be used as antennas for external actuation of interfacial (membrane) properties without causing structural or environmental degradation

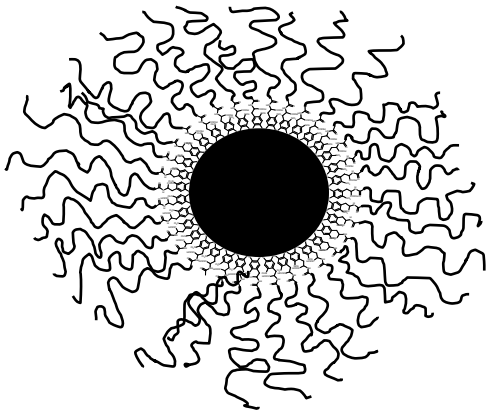

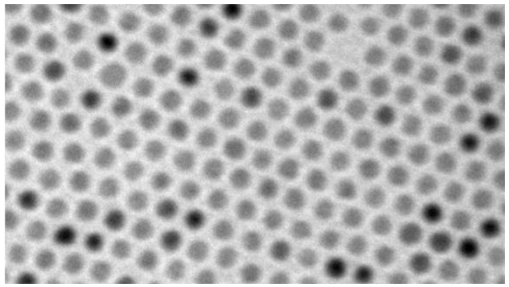

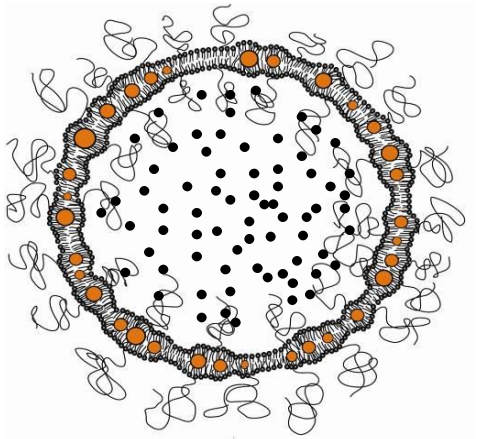

The message today:

- Use the AFM if you get the change, there is a lot of room and also there is a lot of room at the top.

- It is a great technique to „visualize“ molecules, membranes, cells, etc.

- There many theoretical questions to solvem either involving the way we measured or concerning the result interpretation (theory).

- Questions concerning tecnical development are always going on: new measuring modes, combination with other techniques, etc.

A more pleasant message: visit us in Vienna

The microscope and its cousins

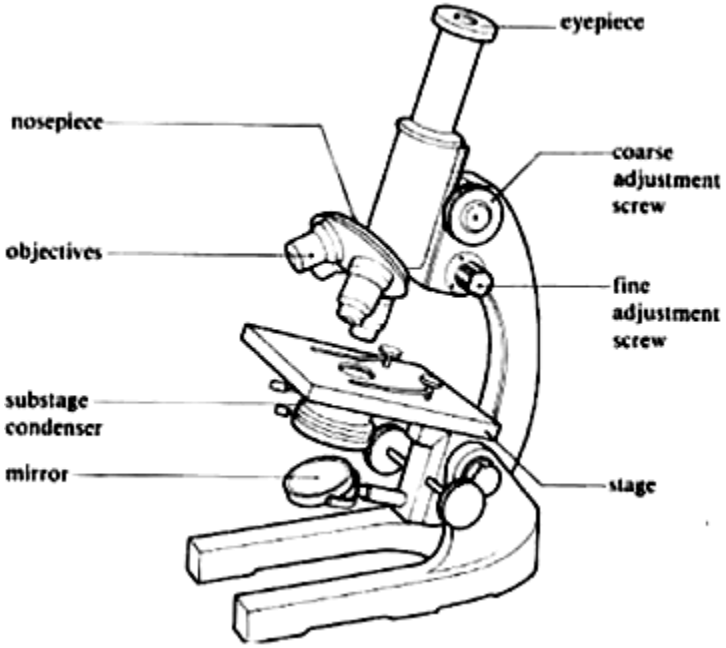

The optical microscope is already old: Salvino D' Armate invented the first eye glasses around 1280

The fluorescence/confocal microscopes are younger…Marvin Minsky developed the confocal around 1957

The resolution depends on the diffraction limit (hundreds of nanometers)

$$r \propto \frac{\lambda}{2n\sin\theta}$$

n: refractive index (1.33 for water)
Lambda: ligth wavelength (400-700 nm, visible)
Theta: aperture angle of the lense

Scanning Probe Microscopy is...

- (a local) surface sensitive technique
- the sensor used has micro-nanometer dimensions

Scanning Probe Microscopy does...

- 3D pictures of sample topology
- Map generation of the sample surface properties
- Interaction forces as a funcion of distance

The AFM...a blind microscope

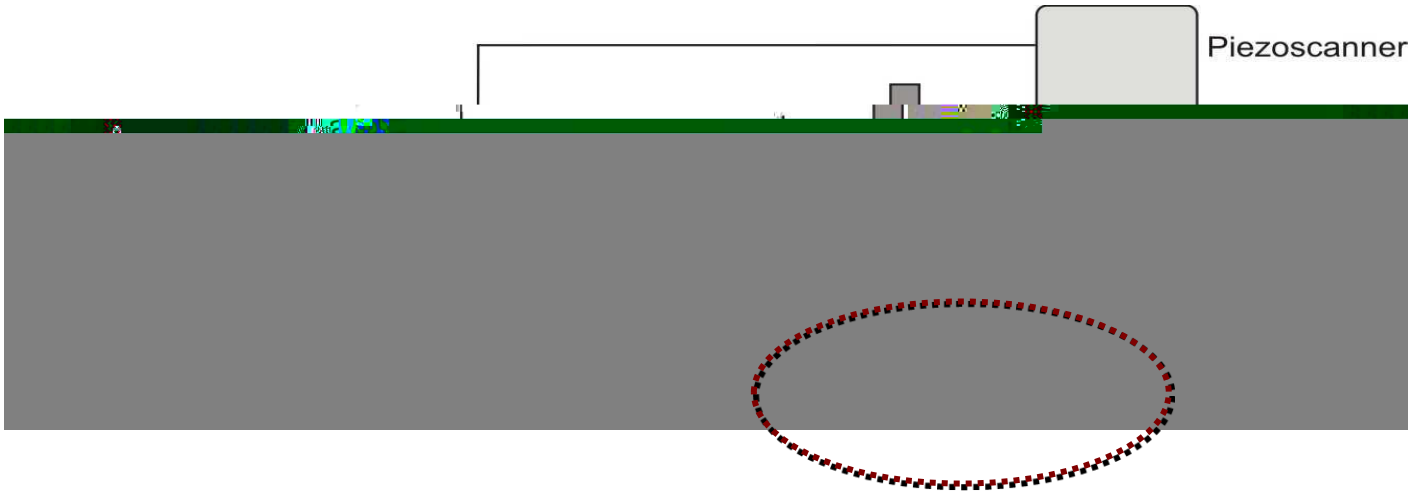

Liquid cell – closed chamber

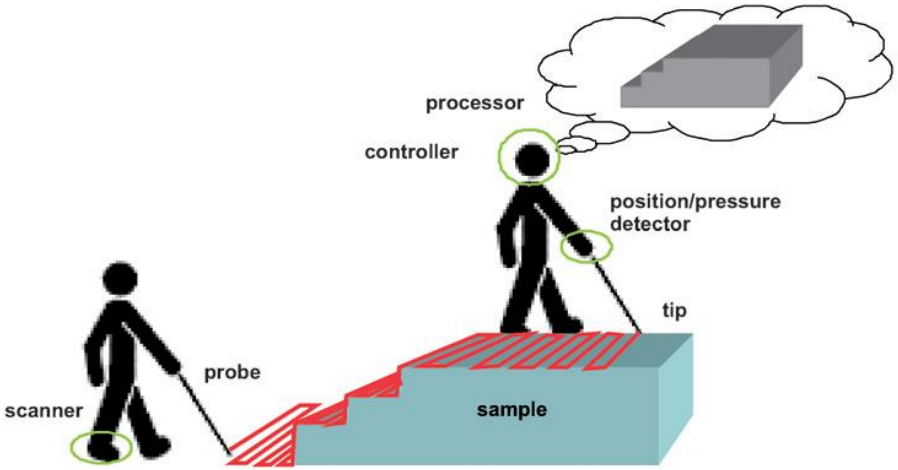

- (Sub)nanometer resolution
- Lower force limit: (dozens of) pN
- You can exchange solvents at different temperatures

Nanoscale 1 (2009) 40

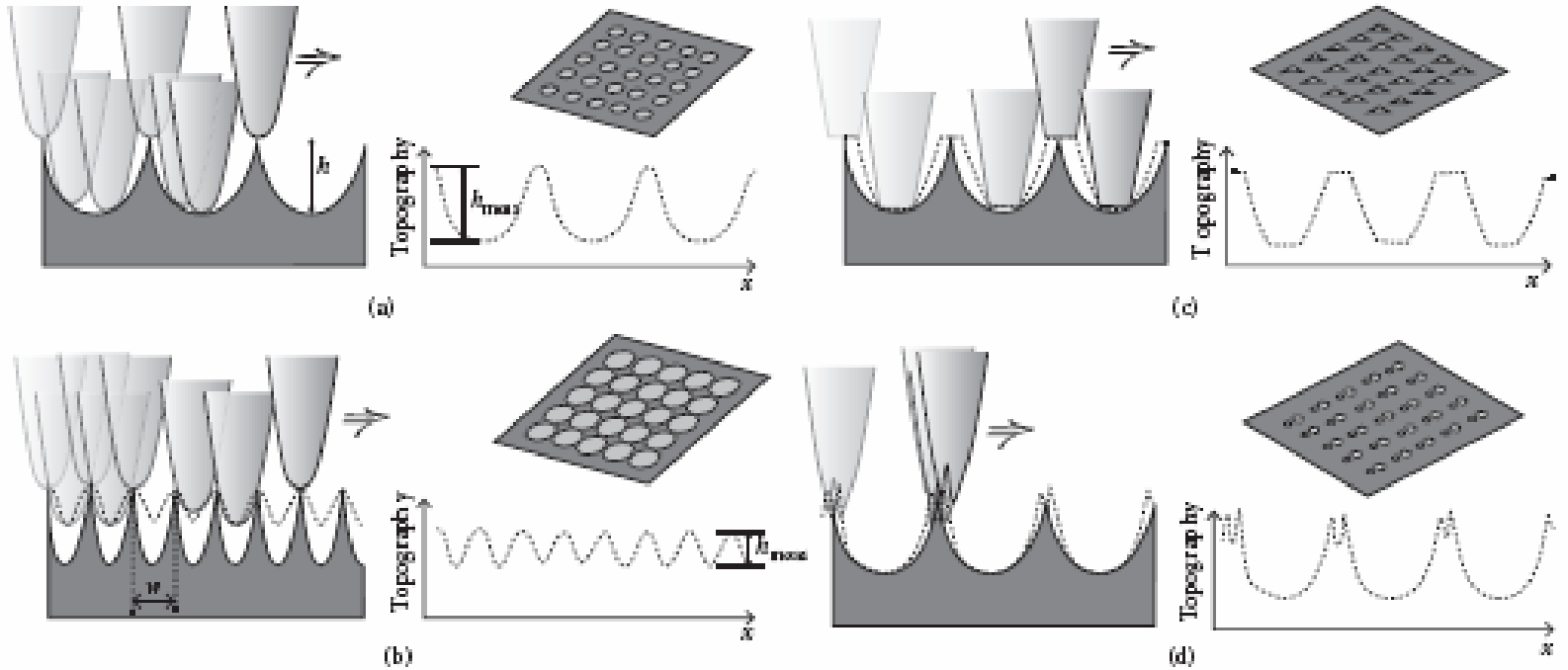

FIGURE 2.18 Some common tip artifacts. (a) Imaging tip shape on sharp sample features. The line profile differs from the sample profile since the curvature radius of the tip is larger than the size of the sample feature. The ordered pattern of spikes appear as round spots in the resulting SPM image. However the measured height (h_{max}) is close to the actual height. (b) If the pattern pitch w is smaller than the curvature radius of the tip, the measured height underestimates the actual height. The spots in the SPM image appear larger and tight to one another. (c) A tapered tip may produce either square or triangular features identically oriented throughout the SPM image. (d) A double-tip probe generates line profiles and images exhibiting doubled features.

Moreno-Flores and Toca-Herrera, *Hybridizing Surface Probe Microscopes*, 2013, CRC Press

AFMs am DNBT... (surface analysis, mechanics and molecular forces)

Scanning probe microscope I

Scanning probe microscope II

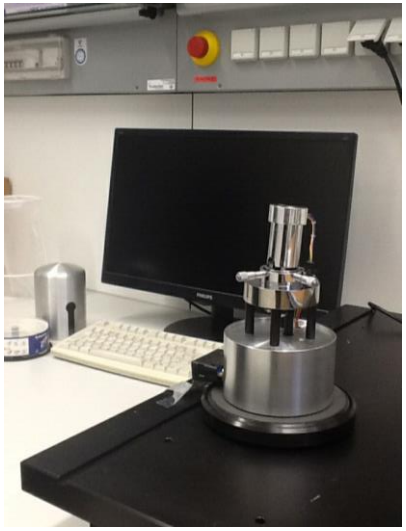

Scanning tunnelling microscope

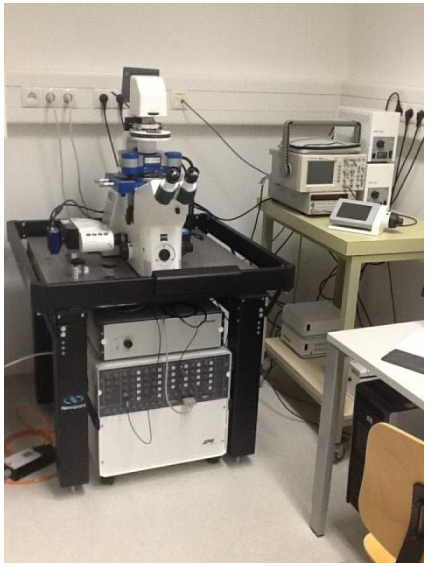

Scanning probe microscope III

Nucleic Acids Research, 1996, Vol. 24, No. 4 713–720

Atomic force microscopy of long and short double-stranded, single-stranded and triple-stranded nucleic acids

Helen G. Hansma*, Irene Revenko, Kerry Kim and Daniel E. Laney

Department of Physics, University of California, Santa Barbara, CA 93106, USA

Received October 5, 1995; Revised and Accepted December 21, 1995

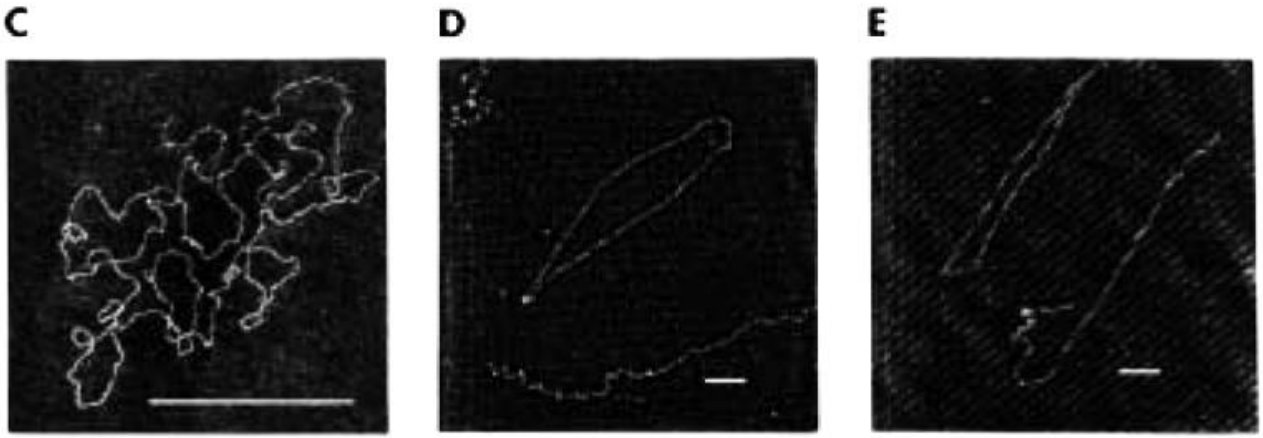

Figure 5. Entire lambda DNA molecules, 48 000 bp on mica. (**A**) Image of a well-extended linear molecule assembled from overlapping AFM images. (**B**) A rare circular molecule. Ethidium bromide (200 ng/μl) was present in the buffer. (**C**) Coiled or tangled molecules such as this one are most common. (**D**, **E**) Entire extended lambda DNA molecules captured in single 10 μm scans. Scale bars 1 μm.

Fibrinogen : an integrin activator

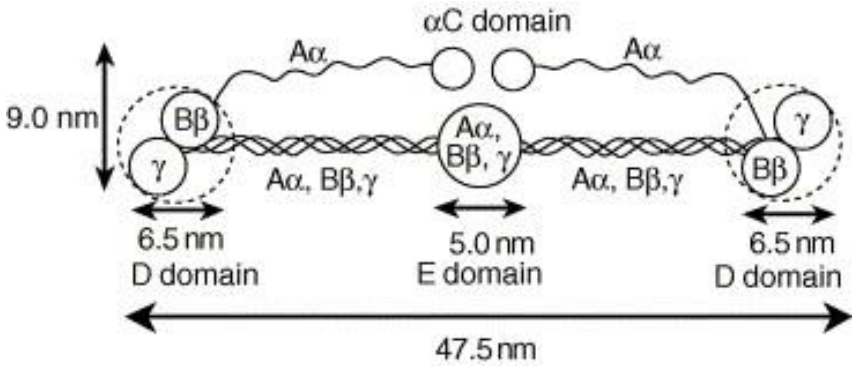

Fibrinogen structure taken from:
Coll. & Surf. B 2007, 57, 89-96

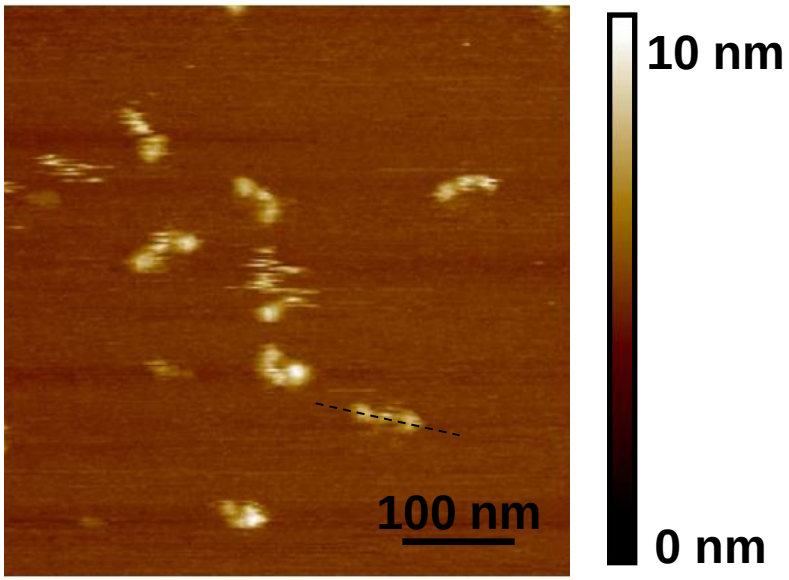

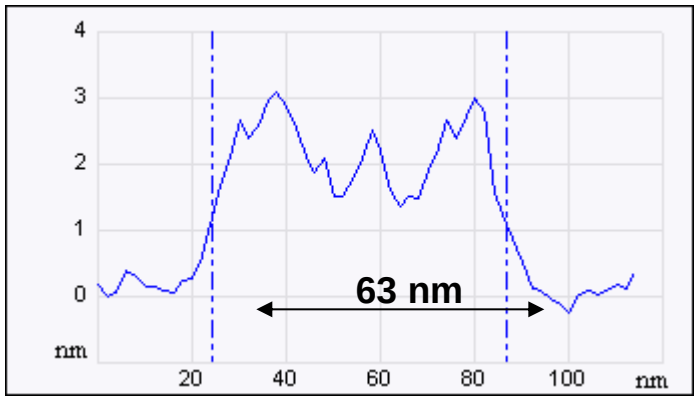

SMF – JLTH, unpublished results

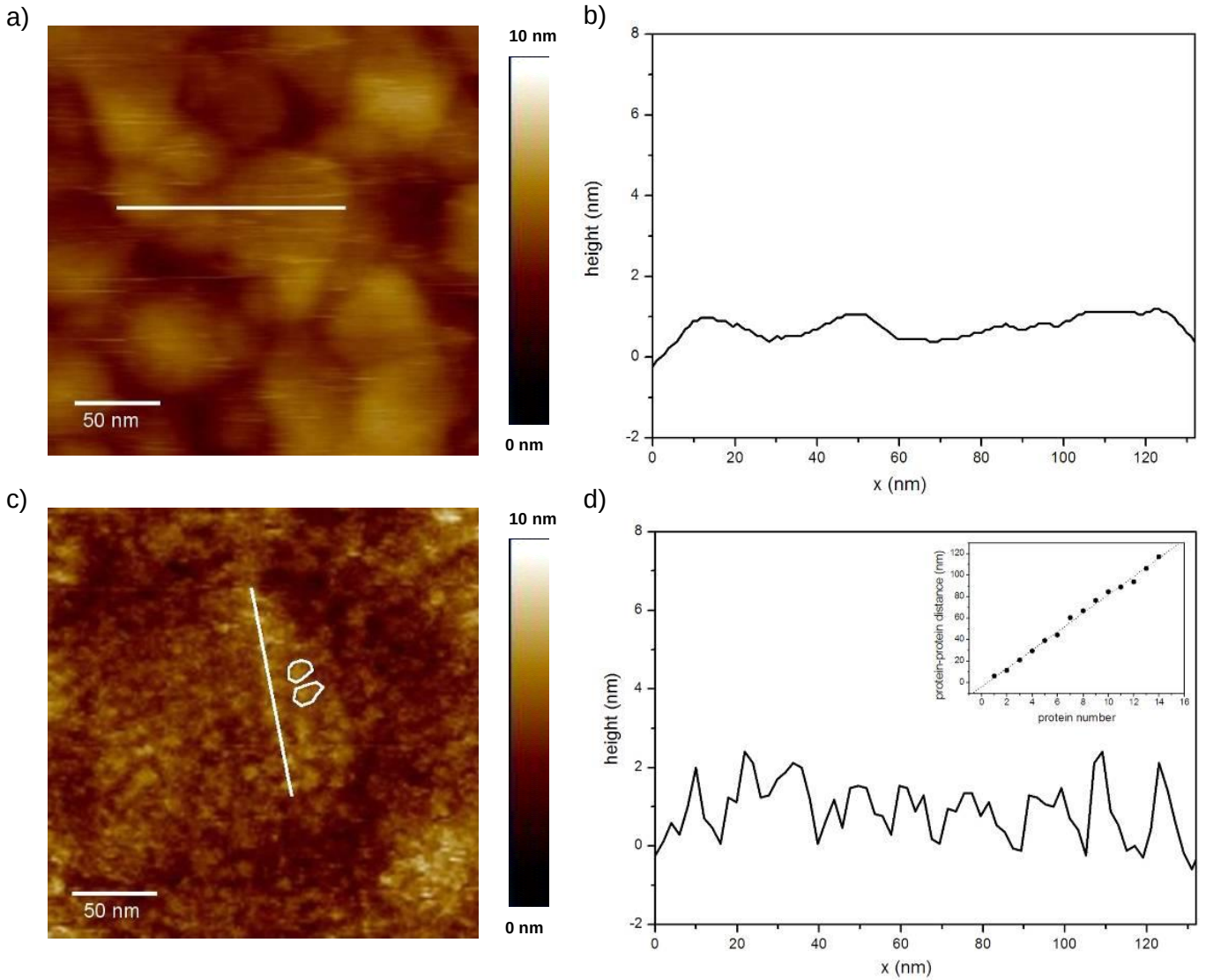

Figure: a) AFM height image (250 x 250 nm^2) of glutaraldehyde functionalized gold substrate. The cross section of its profile is shown in (b).
c) AFM height image (250 x 250 nm^2) of immobilized HSA proteins with glutaraldehyde. The white circles indicate single HSA. The cross section (d) shows that protein-protein Distance is about 8 nm.

Protein crystal formation on SiO_2

SbpA
0.1 mg/ml

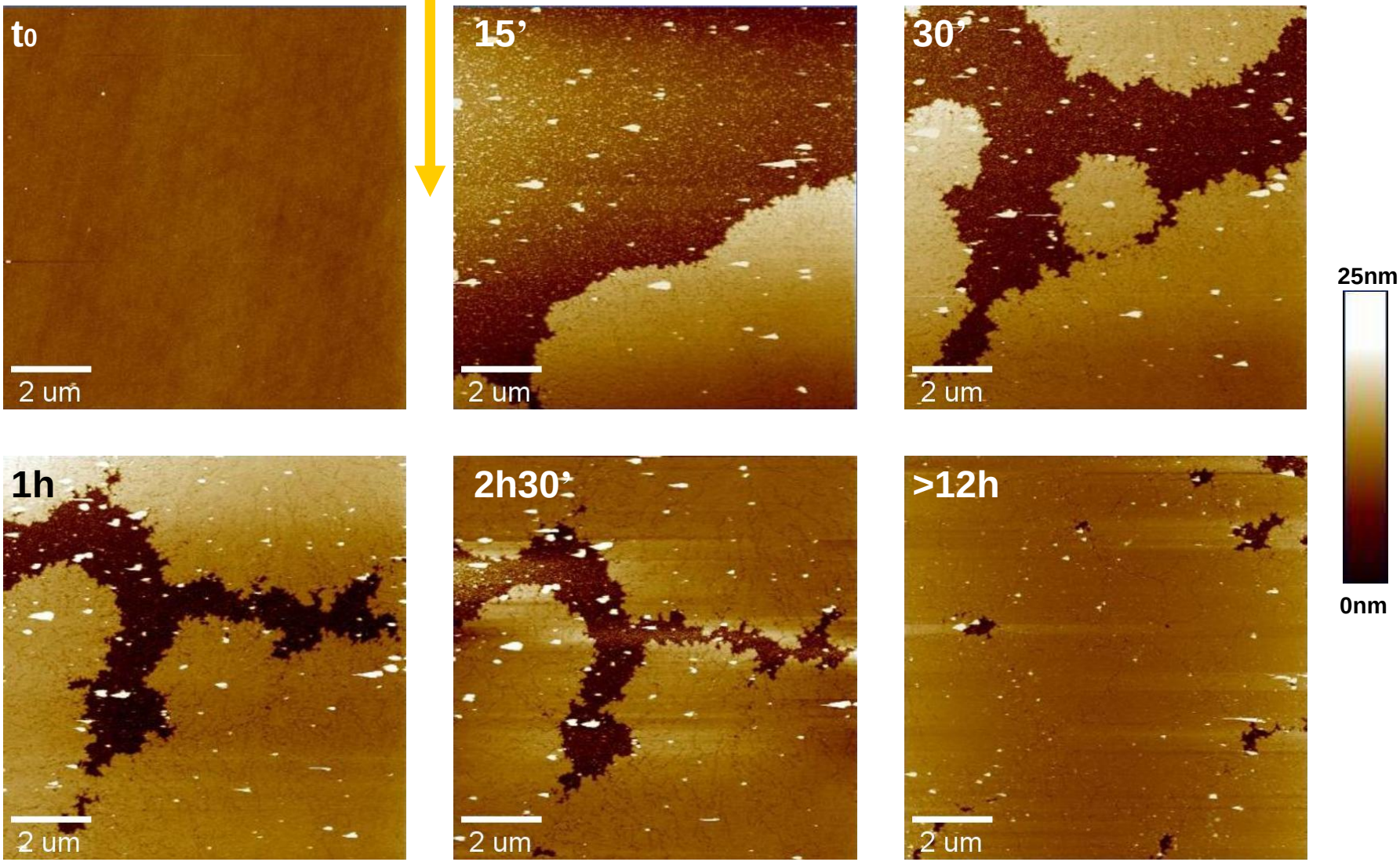

Bacterial crystals on silanes

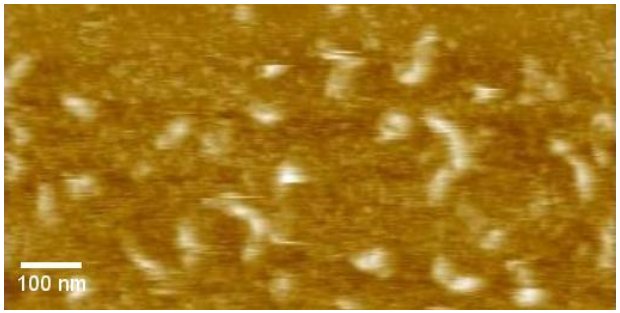

t_0

3^{30}

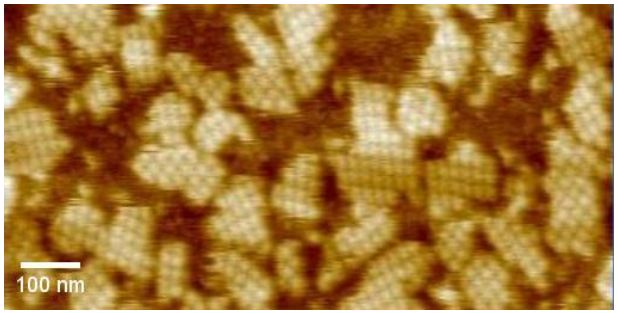

7^{00}

10^{30}

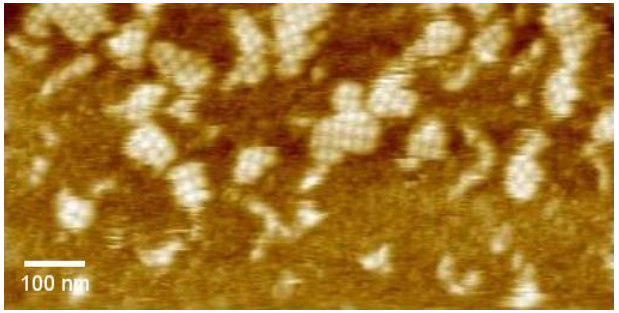

7^{00}

3^{30}

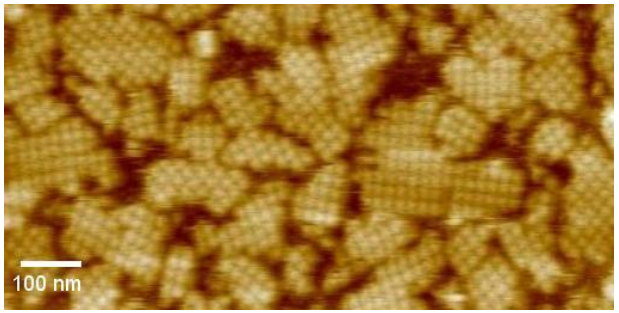

14^{00}

10^{30}

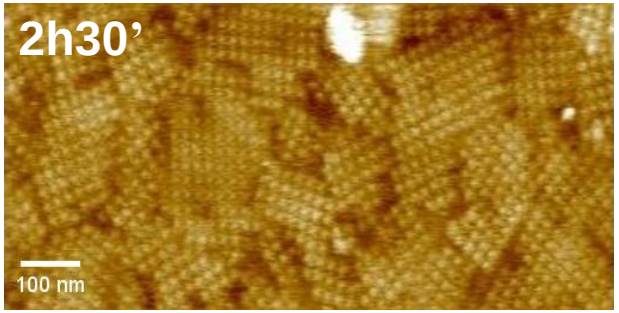

time	SiO_2	OTS	APTS
5’	X	31	21
15’	33	77	68
30’	62	96	83
1h	80	99	85
2h30’	85	99	95
>12h	98	100	100

Small 6 (2010) 40

You can also check thermal stability of protein crystals or polymer brushes

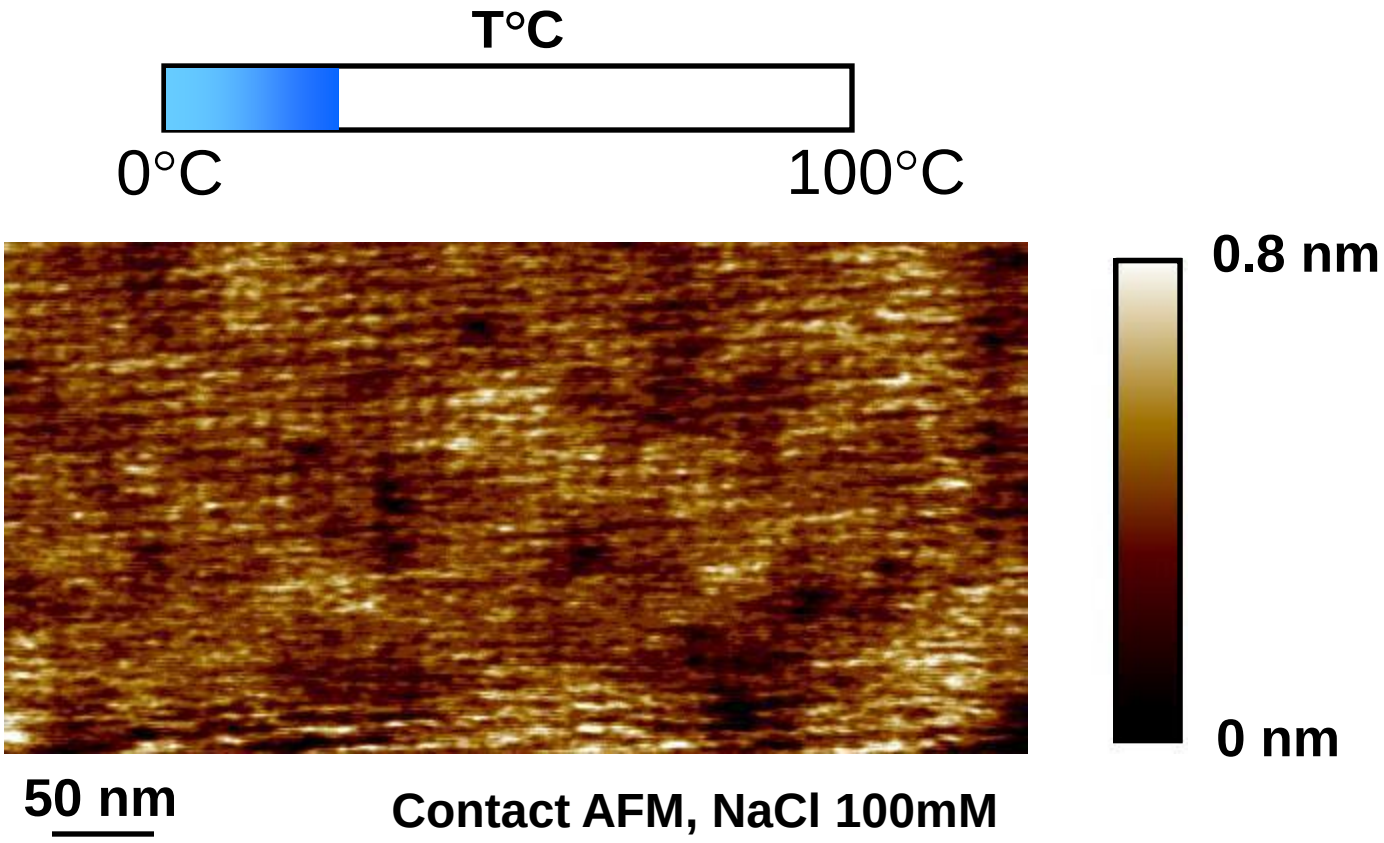

Microscopy Research and Technique 65 (2004) 226

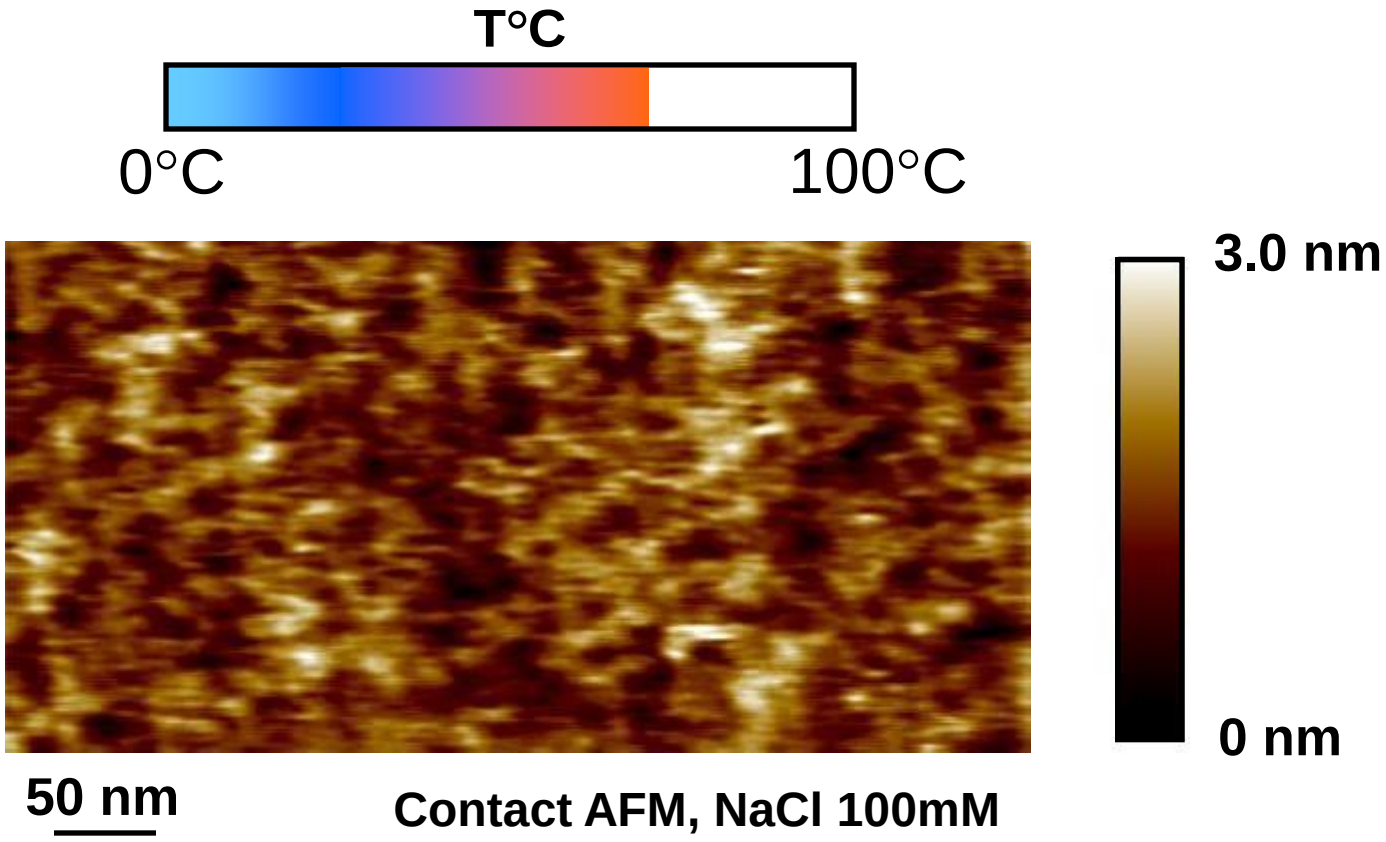
T°C
0°C
100°C
3.0 nm
0 nm
50 nm
Contact AFM, NaCl 100mM

Interaction lipid bilayer / protein toxin

(cooperation with C. Krittanai, Mahidol Univ. Thailand)

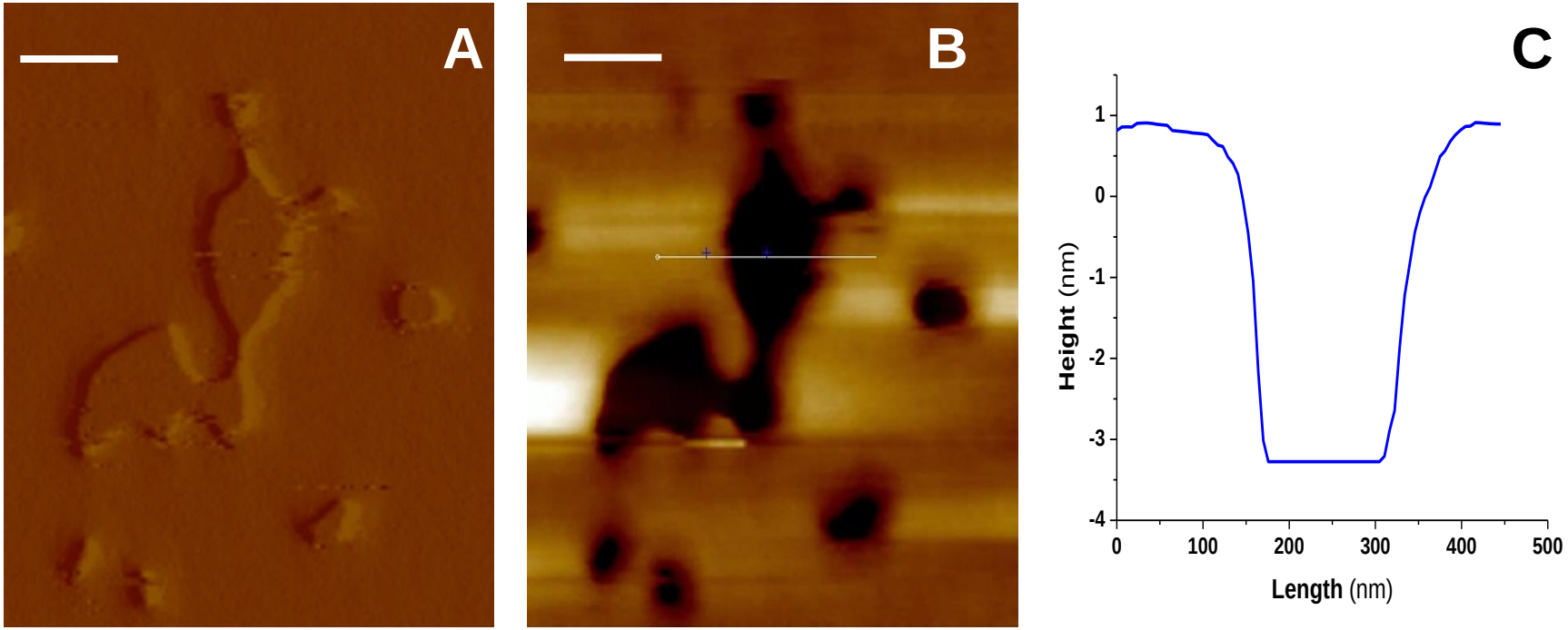

Figure 4. (A) Deflection Error and (B) Height micrographs of a 100 µg/ml Cyt2Aa2 protein film measured in contact mode in the presence of PBS. Scale bars correspond to 200 nm. (C) Height Profile of film defect, as obtained from the arrow drawn in (B).

Submitted to Langmuir, 2015

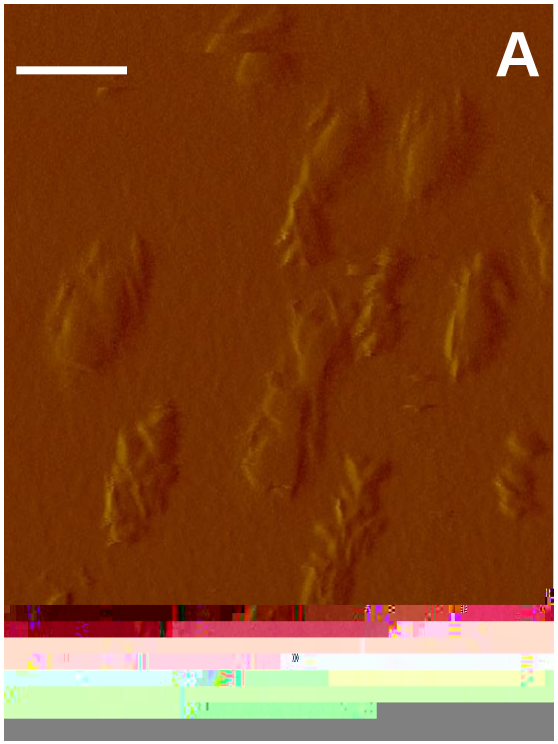

C

Figure 5. (A) Deflection Error and (B) Height micrographs of a 10 µg/ml Cyt2Aa2 protein film measured in contact mode in the presence of PBS. Scale bars correspond to 200 nm. (C) Height profiles, as obtained from the white arrows in (B), corresponding to the width (blue) and length (red) of a protein aggregate.

You can combine AFM with QCM-D: mass adsorption, kinetics, mechanical properties and topography...and maybe to have an explanation.

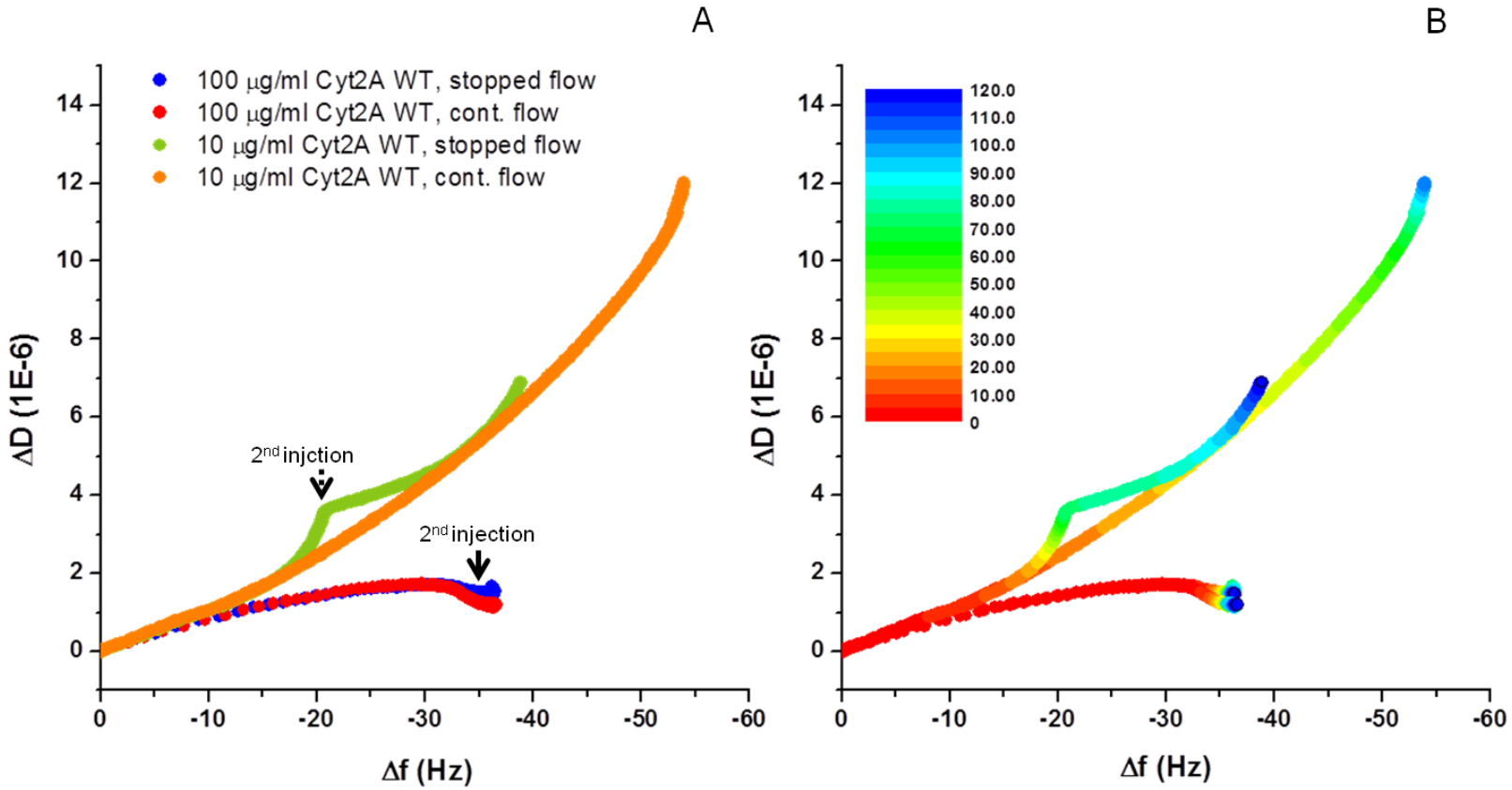

You can combine AFM with QCM-D: mass adsorption, kinetics, mechanical properties and topography...and maybe to have an explanation....

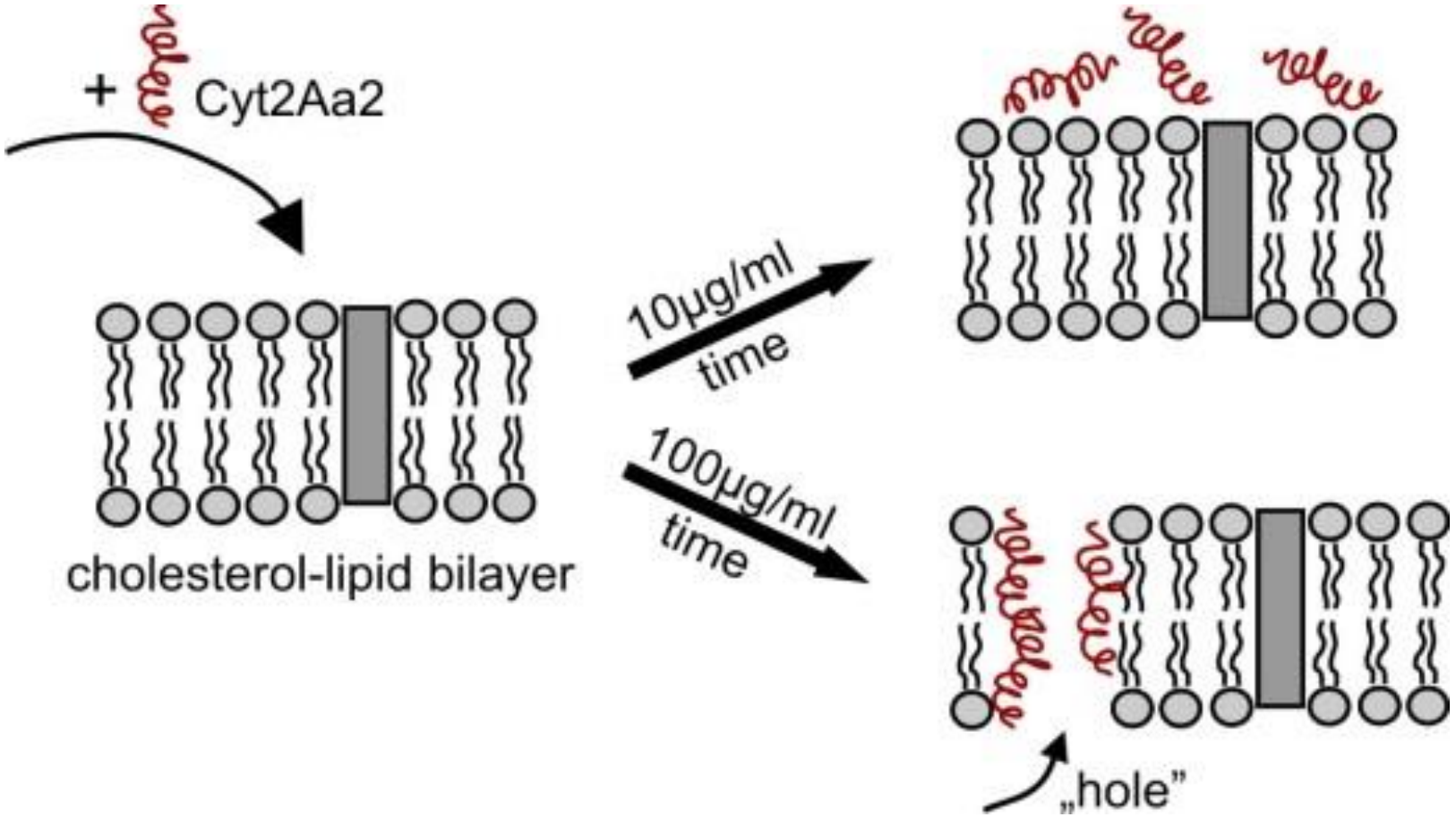

AFM as dynamical „surface force aparatus“ and mechanical indentor

FORCE – DISTANCE CURVES (I)

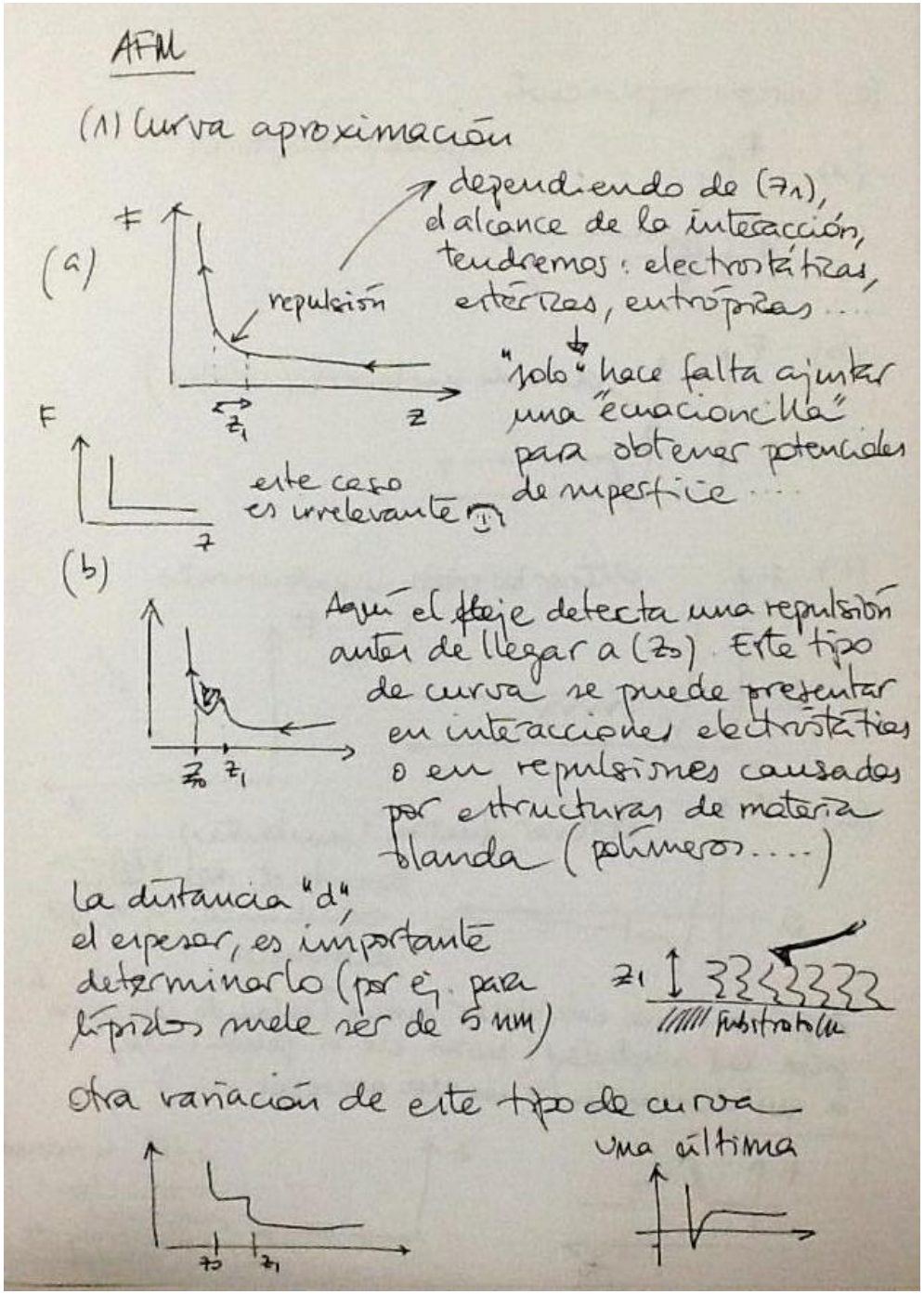

Posibility to explore different Interactions (van der Waals, Electrostatic, hydrophobic, entropic...) and therefore to model them.

FORCE – DISTANCE CURVES (II)

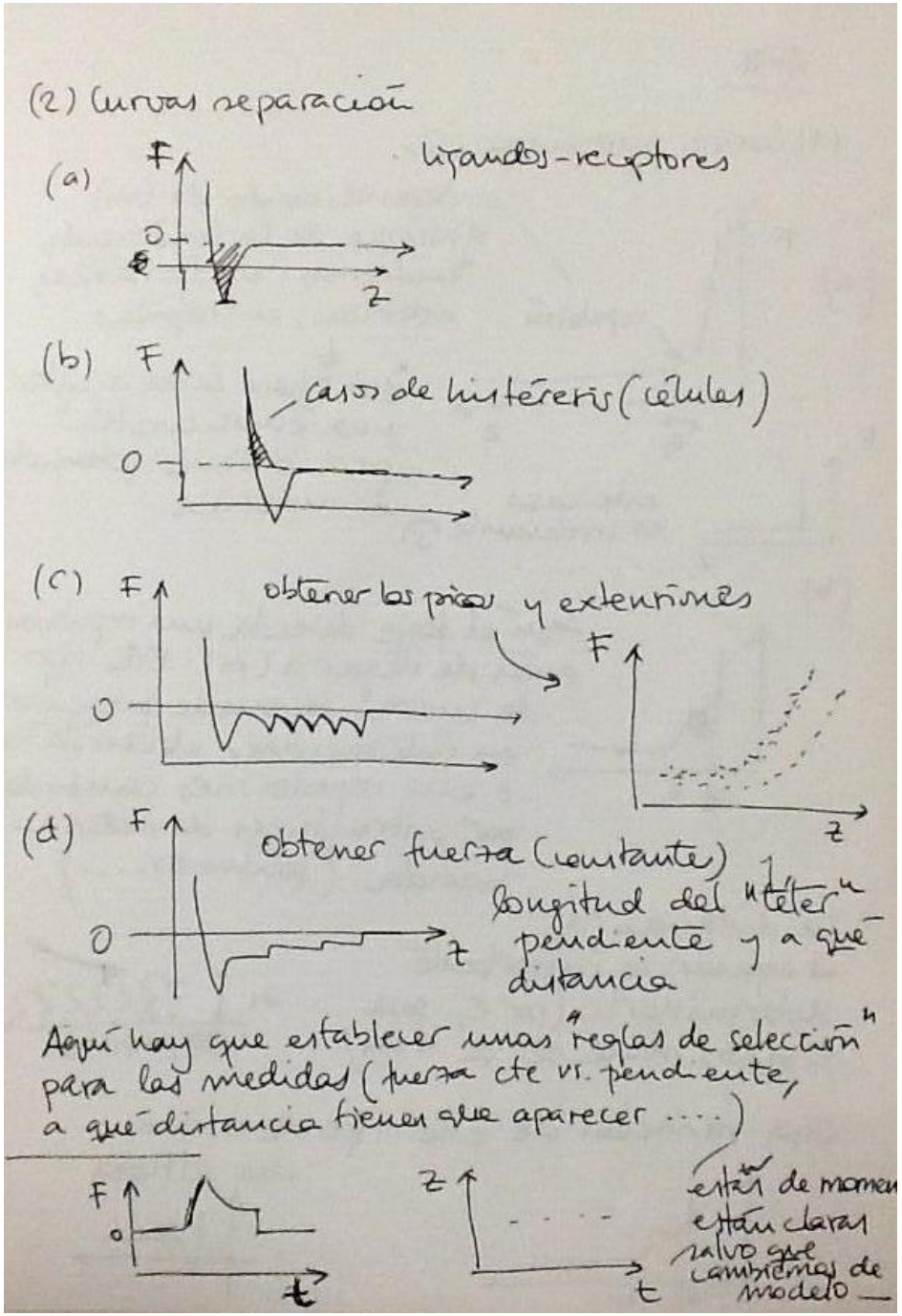

Exploring intramolecular Interactions, mechanical properties of polymers, cells hydrogels.Possibility to test existing theories and to develop „new ones“.

MICROSCOPY RESEARCH AND TECHNIQUE 76:870–876 (2013)

A New Automatic Contact Point Detection Algorithm for AFM Force Curves

RAFAEL BENÍTEZ,[1]* SUSANA MORENO-FLORES,[2,3] VICENTE J. BOLÓS,[4] AND JOSÉ LUIS TOCA-HERRERA[2,3]
[1]*Department of Mathematics, Centro Universitario de Plasencia, University of Extremadura, Avda, Virgen del Puerto 2, 10600 Plasencia, Spain*
[2]*Department of NanoBiotechnology, Institute for Biophysics, BOKU - University of Natural Resources and Applied Life Sciences Vienna (BOKU), Muthgasse 11, 1190 Vienna, Austria*
[3]*Biosurfaces Unit, CIC BiomaGUNE, Paseo Miramón 182, E-20009 San Sebastián-Donostia, Spain*
[4]*Department of Mathematics for Economics, Faculty of Economics, University of Valencia, 46022 Valencia, Spain*

KEY WORDS atomic force microscopy; force measurements; batch processing; automatic contact point detection

ABSTRACT A new method for estimating the contact point in AFM force curves, based on a local regression algorithm, is presented. The main advantage of this method is that can be easily implemented as a computer algorithm and used for a fully automatic detection of the contact points in the approach force curves on living cells. The estimated contact points have been compared to those obtained by other published methods, which were applied either for materials with an elastic response to indentation forces or for experiments at high loading rates. We have found that the differences in the values of the contact points estimated with three different methods were not statistically significant and thus the algorithm is reliable. Also, we test the convenience of the algorithm for batch-processing by computing the contact points of a force curve map of 625 (25×25) curves. *Microsc. Res. Tech. 76:870–876, 2013.*

AFM as a force and mechanical machine: it offers…

- Alternative to conventional methods of denaturation (e.g. heat, acid, chemical denaturant).
- Single molecule experiment.
- Well defined reaction coordinate.
- Direct comparison with all-atom MD simulation.
- Possibility to observe rare events

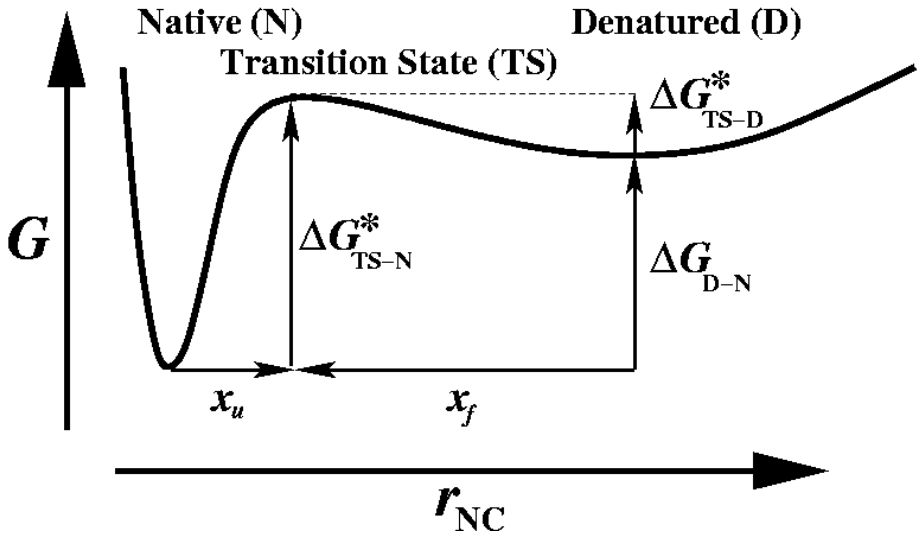

$$k_u(F) = \nu\kappa \exp(-\beta(\Delta G^*_{TS-N} - Fx_u)) = k_u(0)\exp(\beta F x_u)$$

Analytical Chimica Acta, 479 (2003) 87

Specific forces

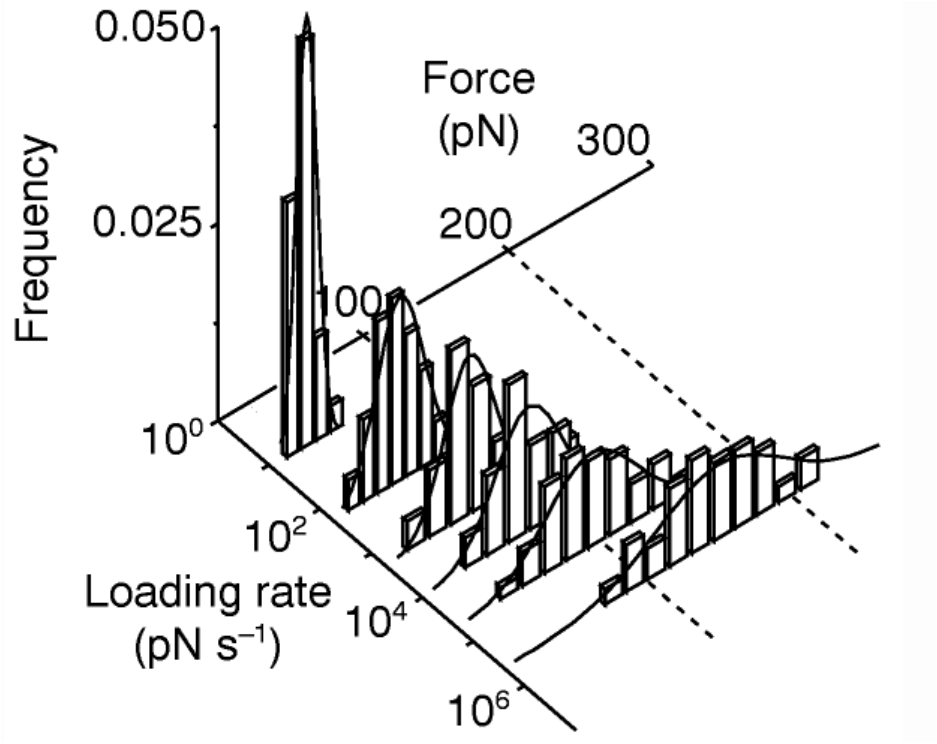

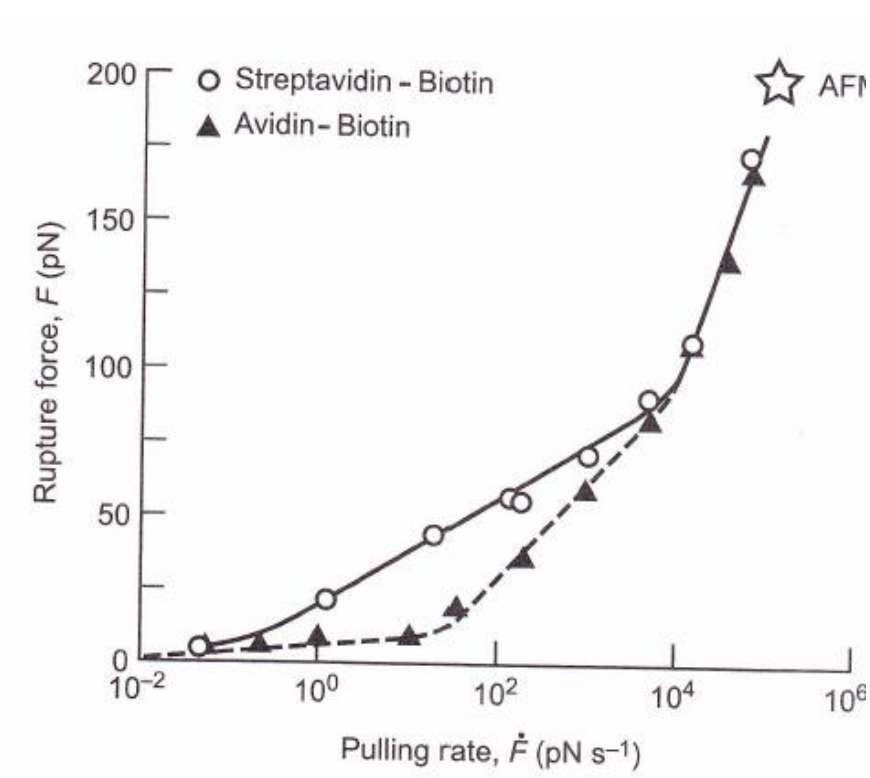

Unbinding forces for streptavidin- biotin and avidin-biotin systems measured with atomic force microscopy as a function of the pulling rate (speed).

Both systems interact via specific forces, that is as ligand-receptor.

Nature 397 (1999) 50

Non-specific forces (albumin – ibuprofen)

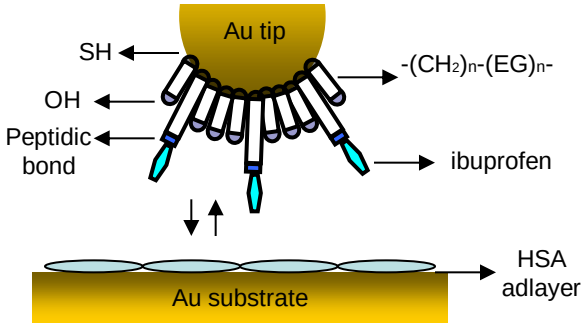

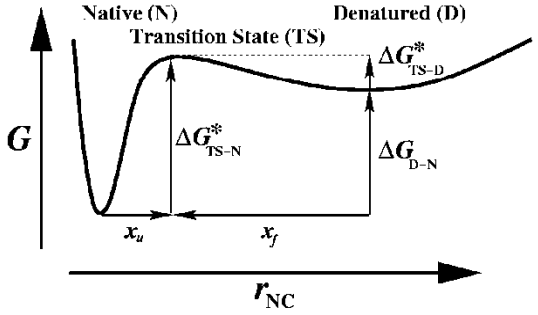

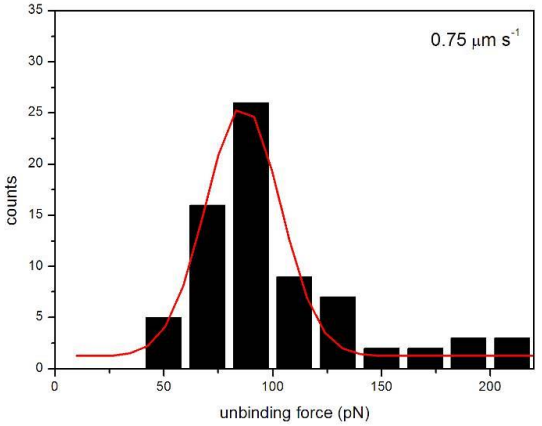

$$F = \left(\frac{k_b T}{x_u}\right)\ln\left(\frac{x_u k_e}{k_b T K_{off}}\right) + \left(\frac{k_b T}{x_u}\right)\ln v$$

X_u = 0.6 nm

K_{off} = 0.055 s^{-1}

Possibility of molecular recognition !!

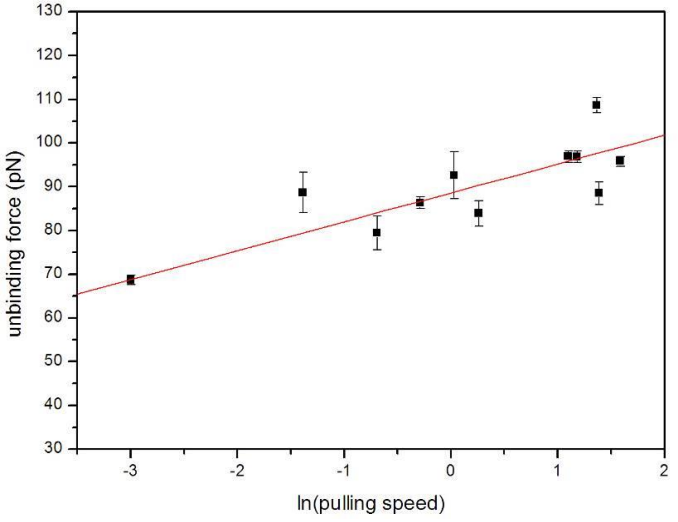

Submitted to Colloids and Surfaces B, 2015

AFM as a mechanical pulling machine on (single) polymers

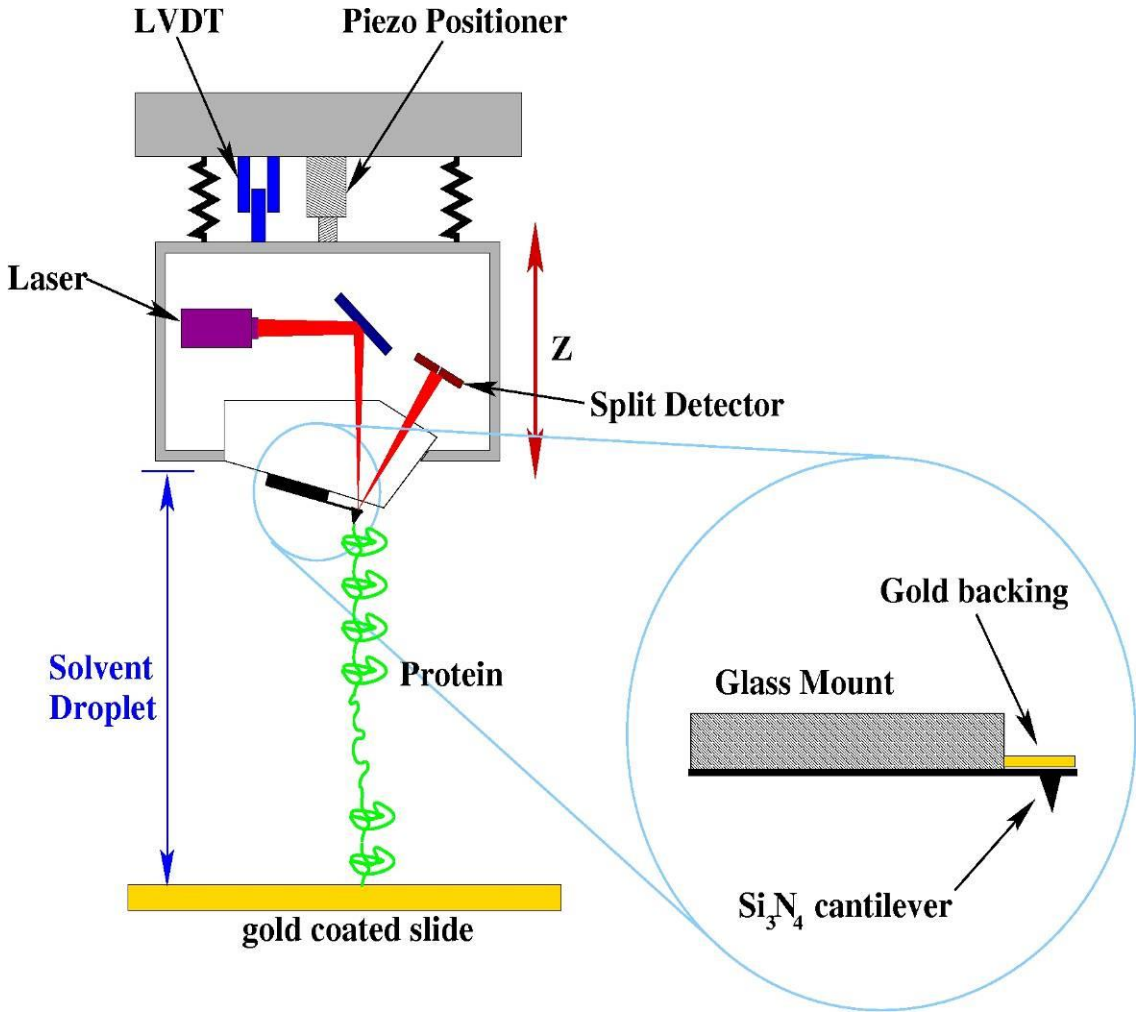

Example: tackling the protein folding problem

Proteins fold into a unique 3-dimensional structure (co-operatively!!!)

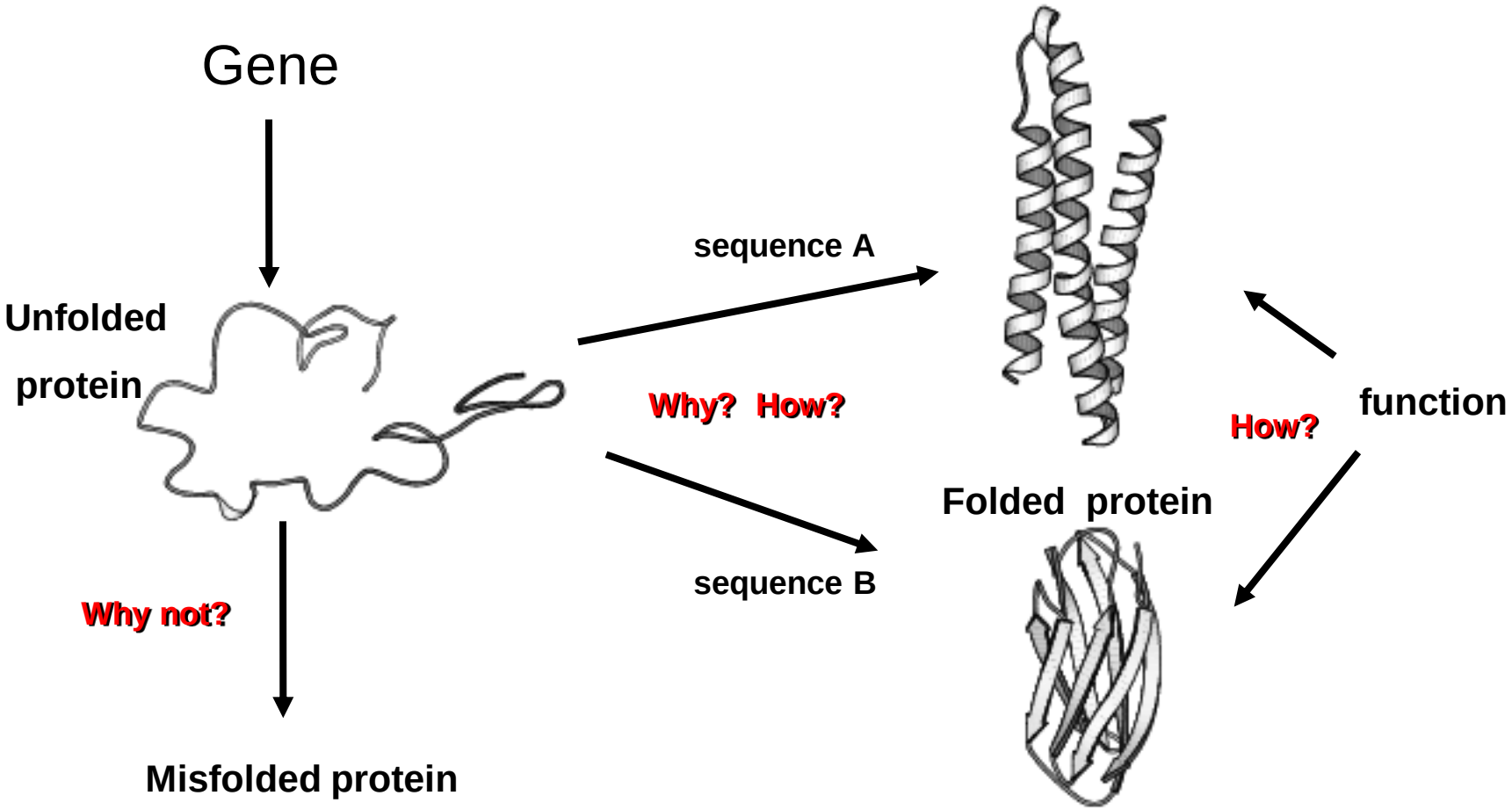

Tenascin and titin I27 have a similar fold: What about their resistance to force?

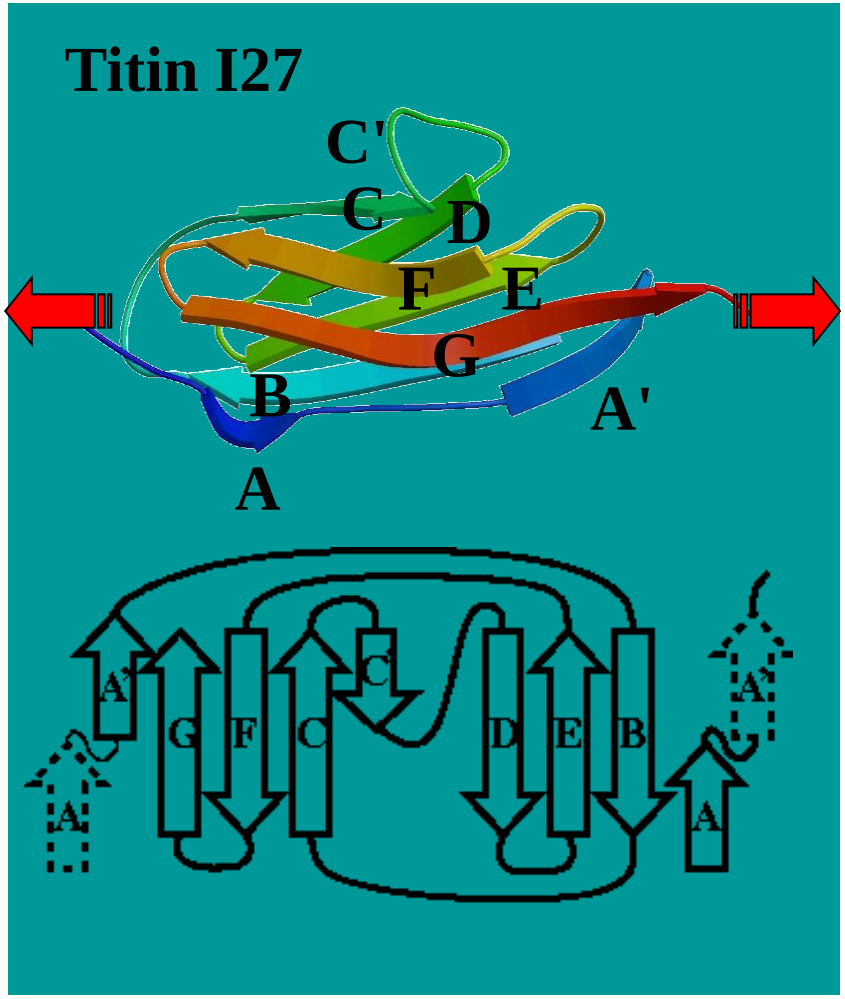

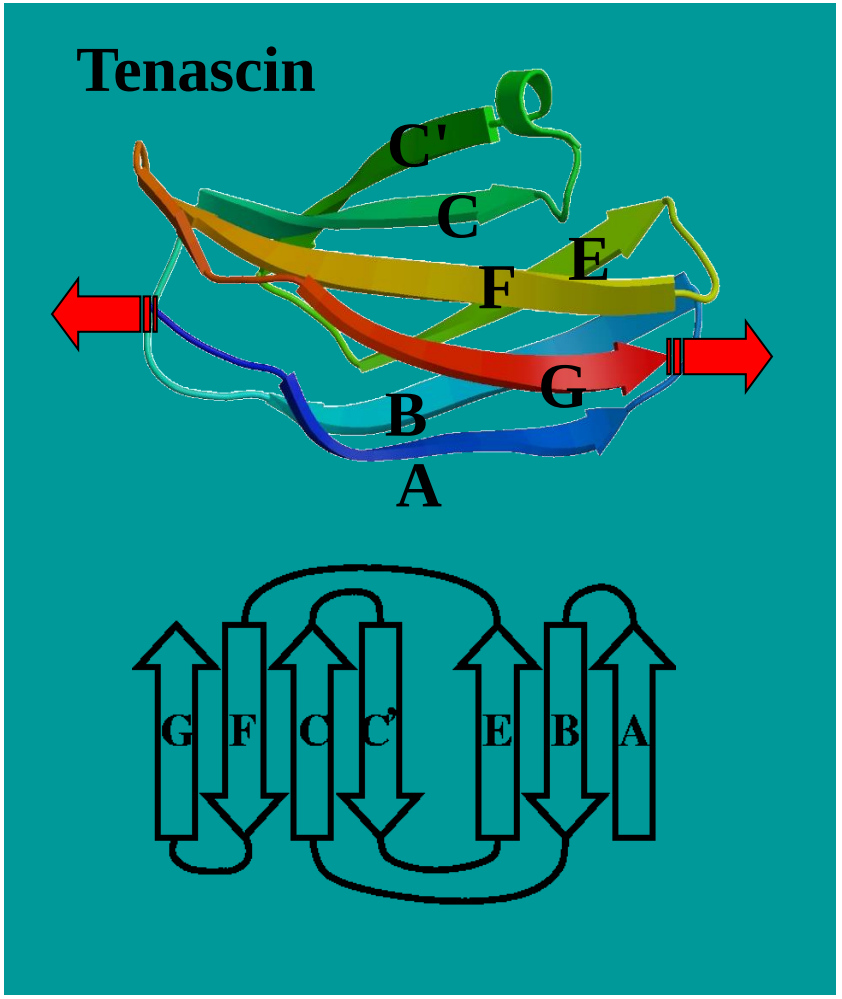

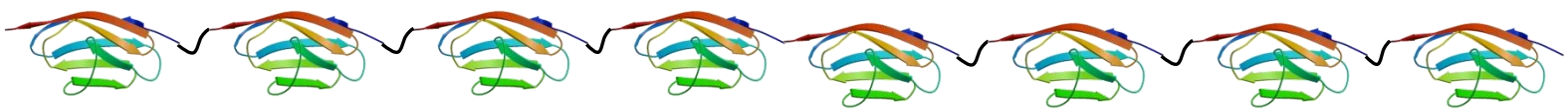

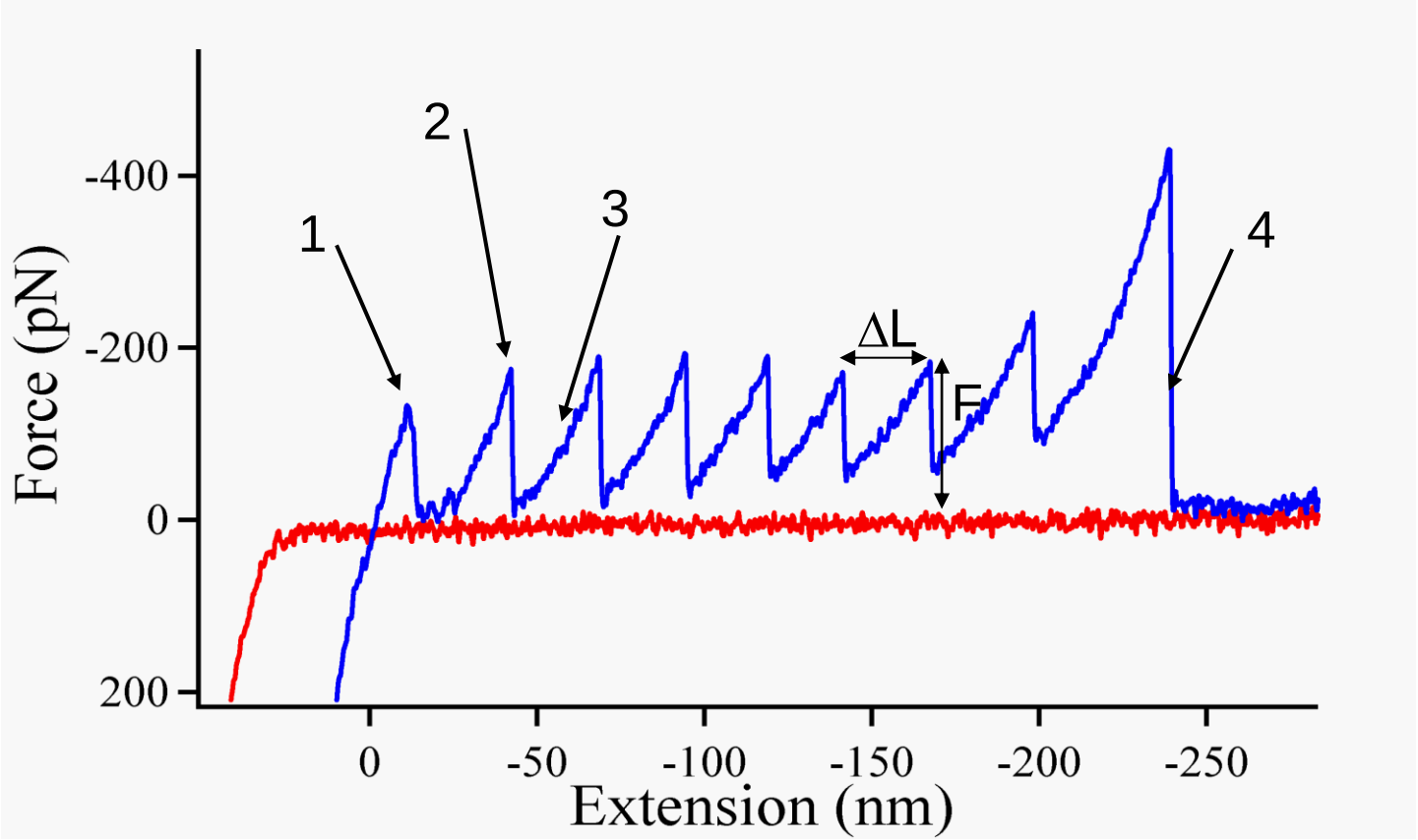

1. Non-specific adhesion 2. Unfolding of one domain

3. Unfolded protein stretching 4. Protein detaches

Interpreting traces: First problem, which ones are the good ones ?

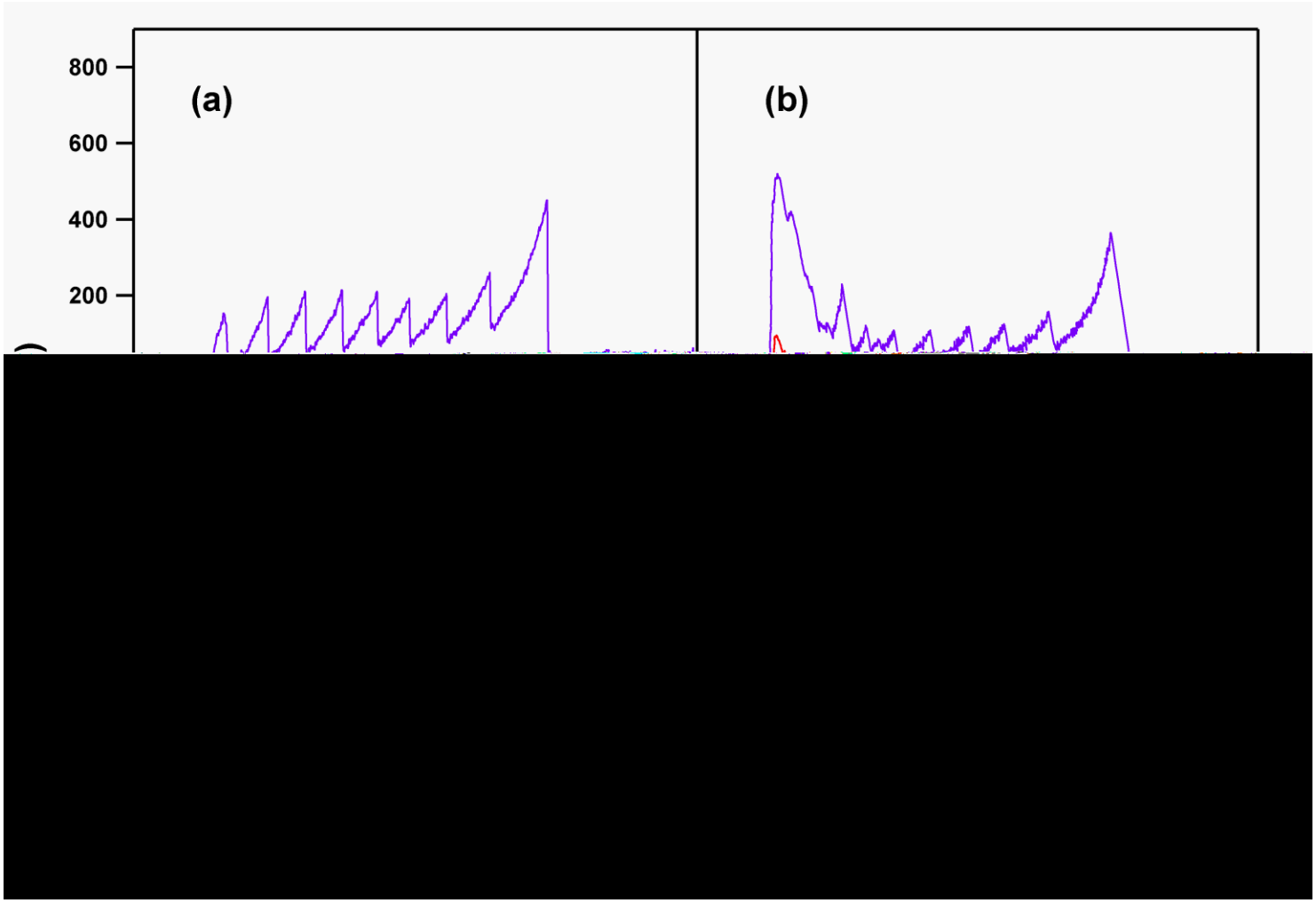

Analytical Chimica Acta, 479 (2003) 87

“Similar” proteins unfold mechanically in a different way

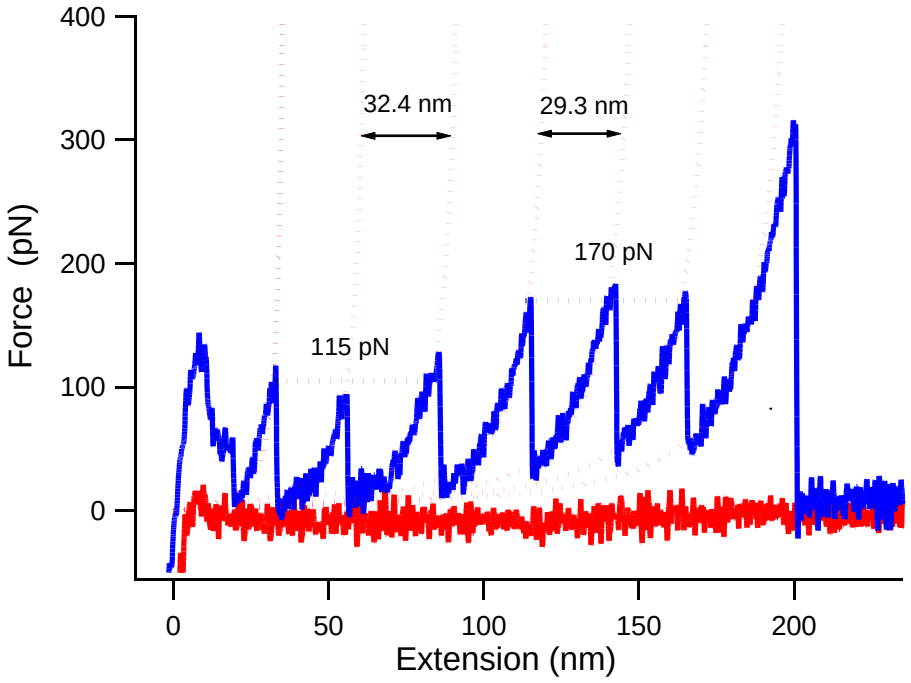

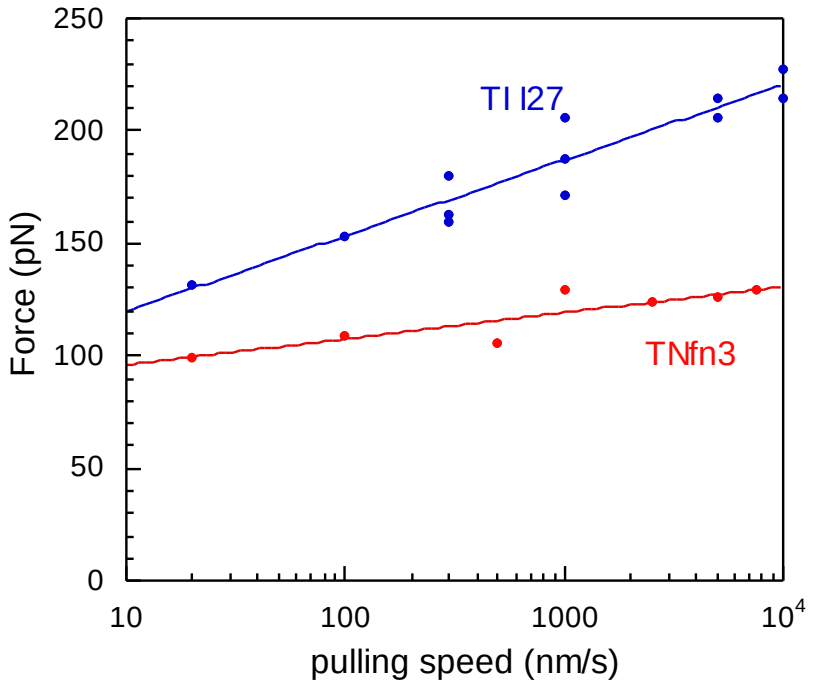

Protein Science, 11 (2002) 2179
Nature, 442 (2003) 446

Experimental limitations: need for MC and MC

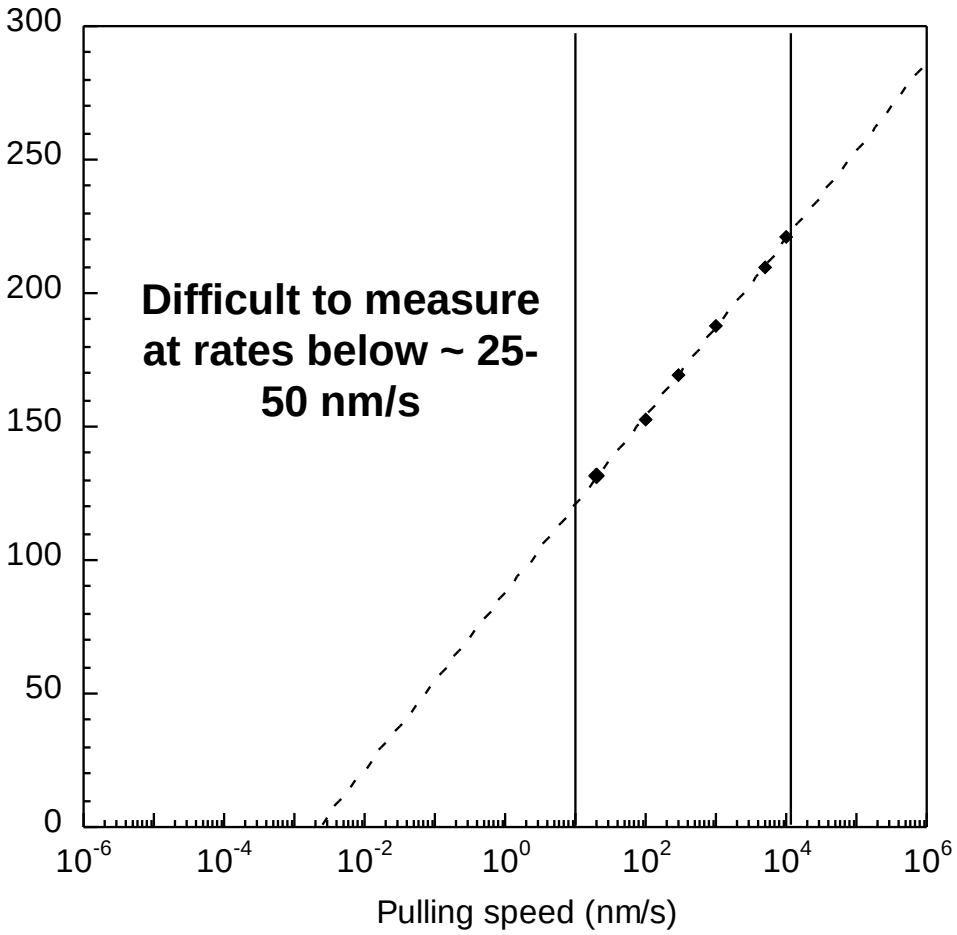

PNAS 99 (2002) 12143

AFM as (dynamical) mechanical indentor

AFM as compressing mechanical machine on lipid bilayers, polymer brushes, hydrogels, cells…

Local deformation

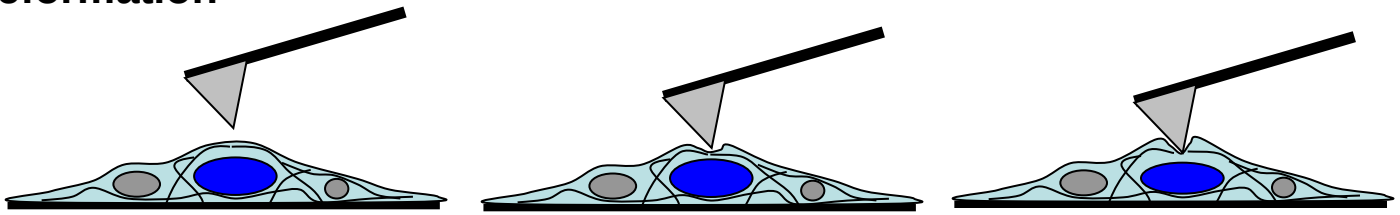

Global deformation

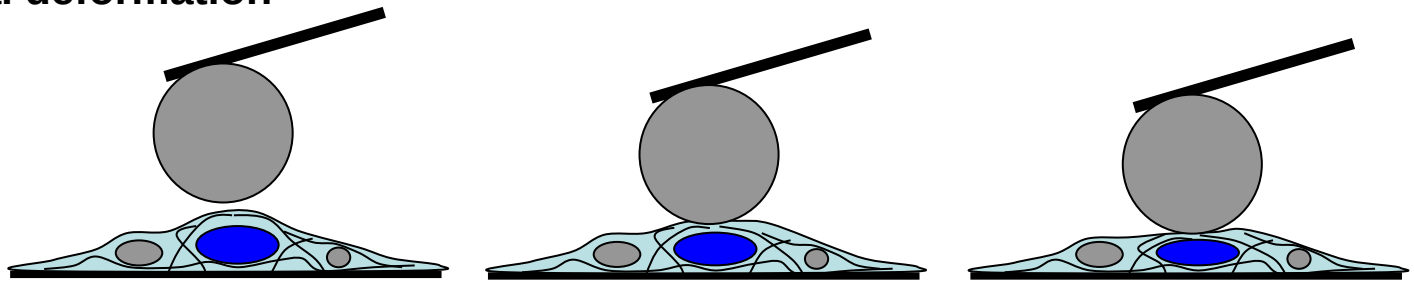

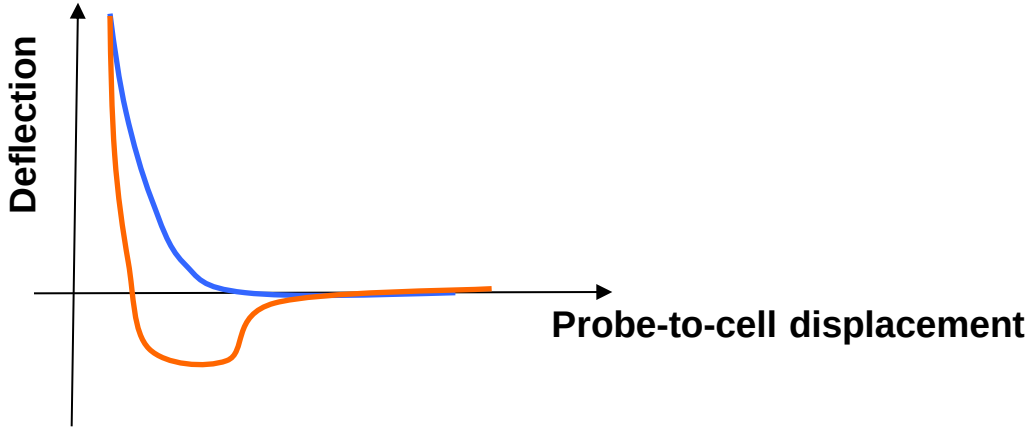

Force-distance based approach: molecular interactions, biomaterials elasticity

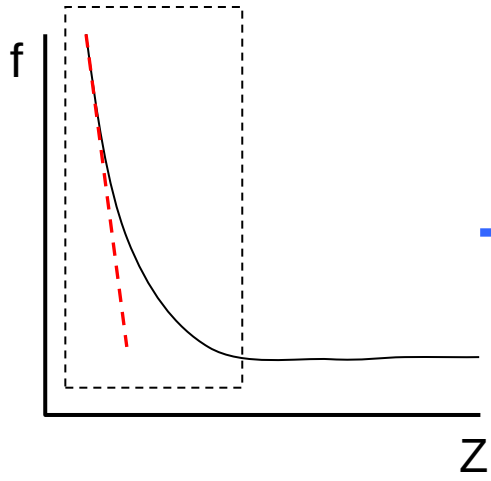

+ **CONTACT AREA [contact mechanics of a purely elastic body]** = **YOUNG'S MODULUS [elasticity parameter]**

- small deformations (1-5%)

- cells = purely elastic bodies

$$F = Cte * E * I^2$$

Every tip shape has its model....

TABLE 7.3

Summary of the Available Theories That Describe the Contact Mechanics of Elastic Bodies

MODELS	GEOMETRY	FORCE-INDENTATION ($F=f(\delta)$, $\delta=f(F)$)	APPLICATION
Hertz		$F=\frac{8GR^{1/2}}{3(1-\nu)}\delta^{3/2}$	- continuum theories - mesoscopic scale: van der Waals (vdW), adhesion and capillary forces are negligible - soft-elastic surfaces - the flat surface is a half-infinite space - tip-sample forces outside the contact area are **not** considered
Sneddon		$F=\frac{4G\delta}{1-\nu}$	
		$F=\frac{4G\cot\alpha}{\pi(1-\nu)}\delta^2$	
		$F=\frac{8G}{3(1-\nu)}a\delta$ a = contact radius	
		$F=\frac{G\pi}{(1-\nu)\beta}[(a^2+\beta^2)\log\frac{\beta+a}{\beta-a}-2a\beta]$ a = contact radius	
Bilodeau		$F=\frac{1.4906G\cot\alpha}{(1-\nu)}\delta^2$	
DMT		$F-F_{adh}=\frac{8GR^{1/2}}{3(1-\nu)}\delta^{3/2}$	vdW forces in the contact area; large probes; high adhesion; stiff samples — tip-sample forces outside the contact area are **not** considered
JKR		$\delta=\frac{2}{3}\sqrt[3]{\frac{(1-\nu)F_{adh}a}{8GR}}$ $a=\sqrt[3]{\frac{3R(1-\nu)}{8G}[F+\frac{3}{2}F_{adh}+(3F_{adh}F+(\frac{3}{2}F_{adh})^2)^{1/2}]^{1/3}}$	short-range forces in the contact area; large, low-stiffness probes; high adhesion; soft samples — tip-sample forces outside the contact area are **not** considered
Maugis and Pollock		$F=\bar{A}^2\lambda\bar{\lambda}^2[\sqrt{m^2-1}+\arctan\sqrt{m^2-1}]$ $\bar{\delta}=\bar{A}^2-\frac{4}{3}\lambda\bar{\lambda}\sqrt{m^2-1}$ $\bar{F}=\frac{2F}{F_{adh}}$ $\lambda=\frac{4.2.06}{D_0}\sqrt[3]{\frac{9F^2_{adh}(1-\nu^2)^2}{4\pi^2RG^2}}$ $\bar{\delta}=\frac{4\delta}{\sqrt[3]{\frac{9F^2_{adh}(1-\nu^2)^2}{4RG^2}}}$ $\bar{A}=\frac{2a}{\sqrt[3]{\frac{3RF_{adh}(1-\nu)}{2G}}}$	- generalized, parametric expressions - large and small probes, large and small adhesion forces - tip-sample forces outside the contact area are considered - m = ratio of contact radius a to an annular region around that contributes to the adhesion parameter λ $\lambda \to$ infinite => JKR $\lambda \to 0$ => DMT

Moreno-Flores and Toca-Herrera, *Hybridizing Surface Probe Microscopes*, 2013, CRC Press

Indenting lipid (cholesterol) bilayers

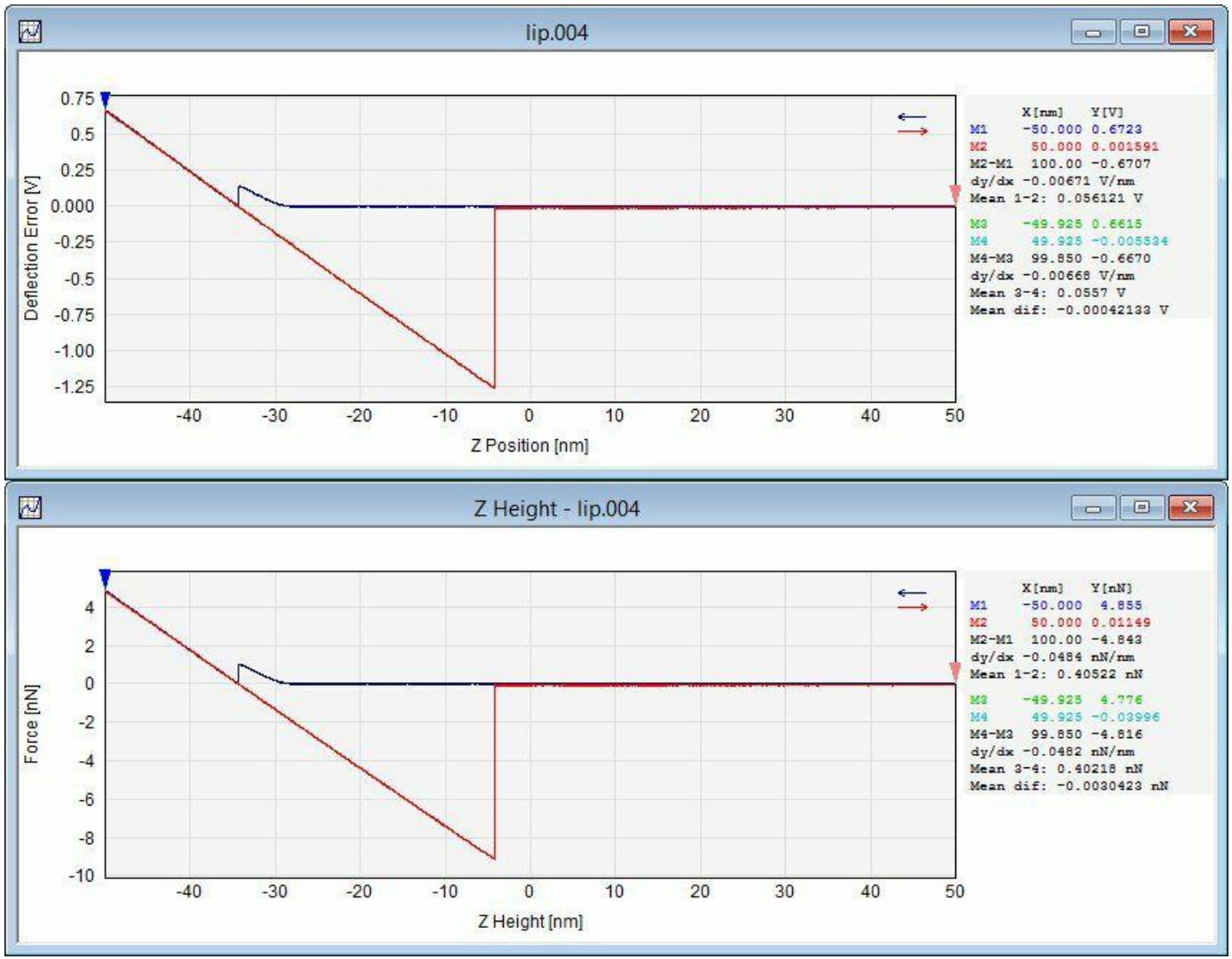

AFM – mechanical machine on cells: preliminaries

1993

Weisenhorn *et al*

Force-indentation of lung carcinoma cells

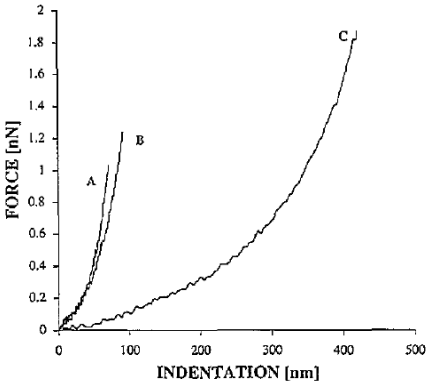

1996

Radmacher *et al*

Human platelet elasticity

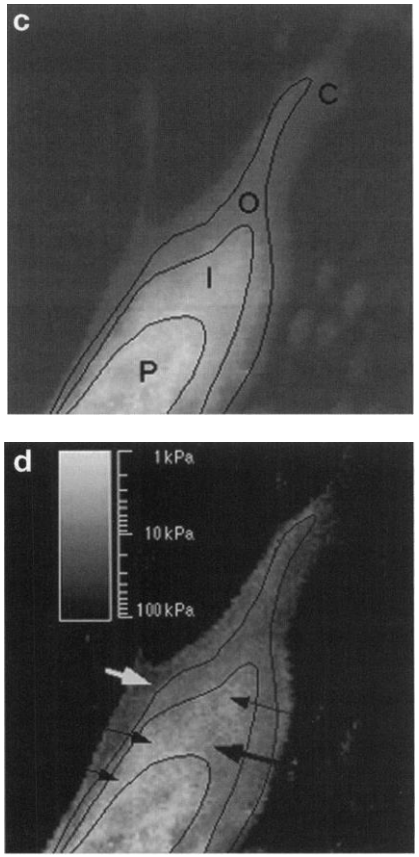

2000

Langer *et al*

Mechanical estimulation of choclear cell stereocilia

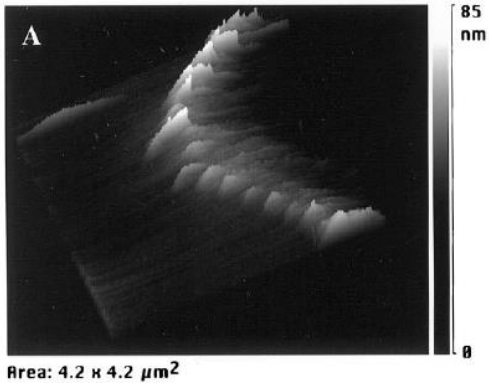

Force-distance curves: surface charge influences the mechanical properties - HepG2 cells

PEI

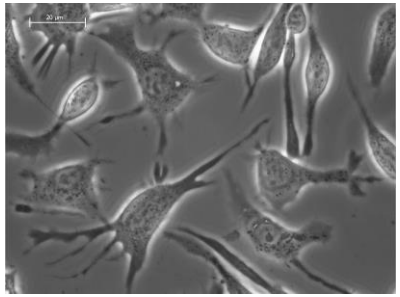

PSS

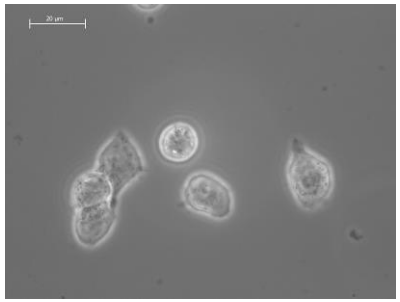

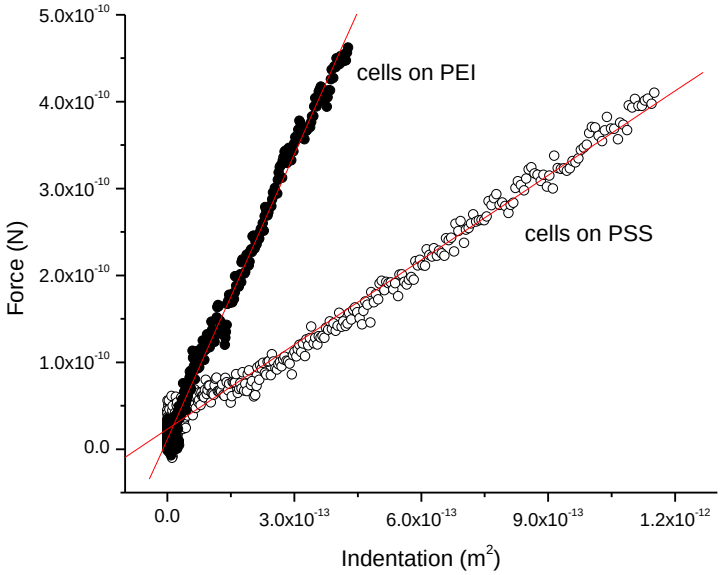

- small deformations
- cells = purely elastic bodies
- 191 ± 14 Pa (PSS, anionic)
- 941 ± 58 Pa (PEI, anionic)

Microscopy Research and Technique 72 (2009) 957

Making RBC look younger – inducing cell shape change

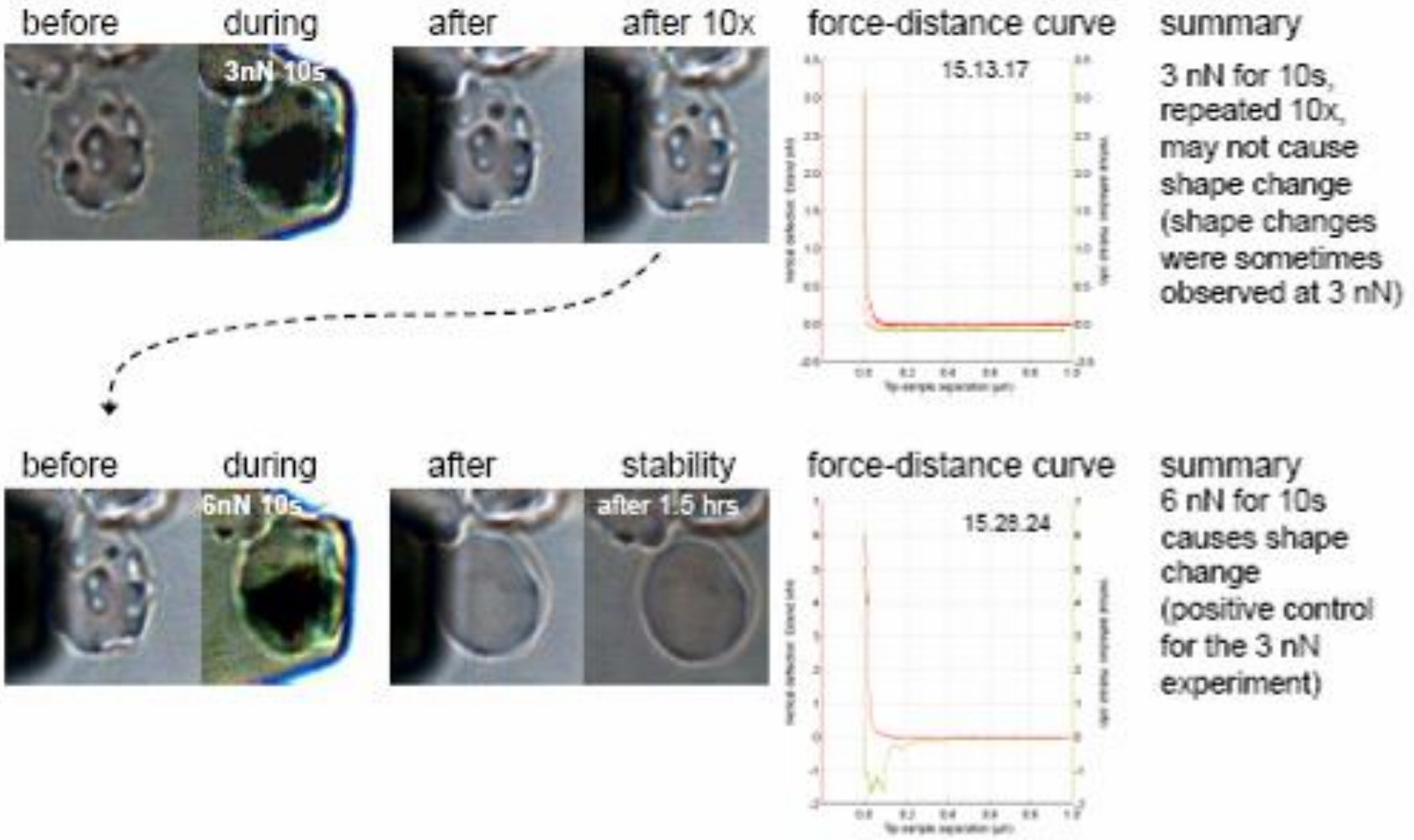

Soft Matter 8 (2012) 3716

Membrane energy is a function of:
the membrane curvature, the area difference between the two membrane leaflets, and cytoskeleton deformation.

Minimisation of the membrane energy causes the lipid translocation, with the relaxation of the cytoskeleton being an additional driving force.

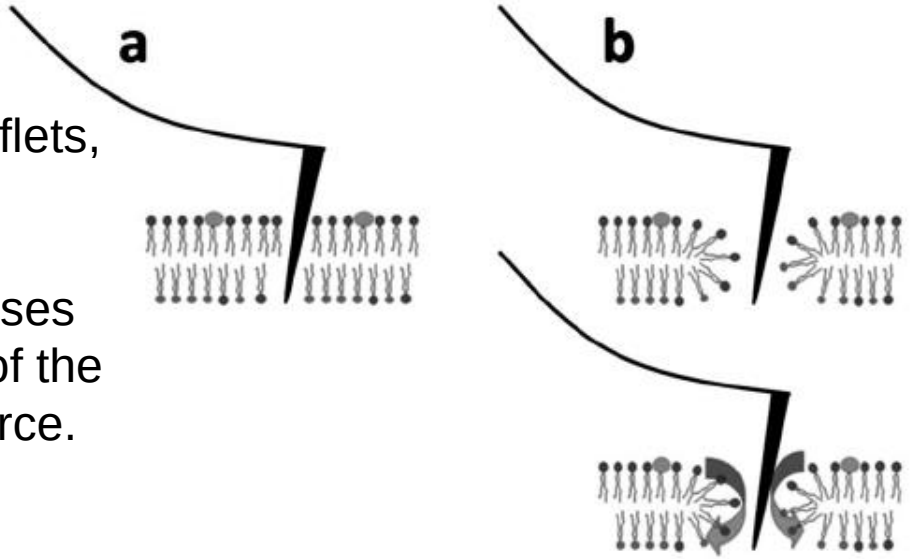

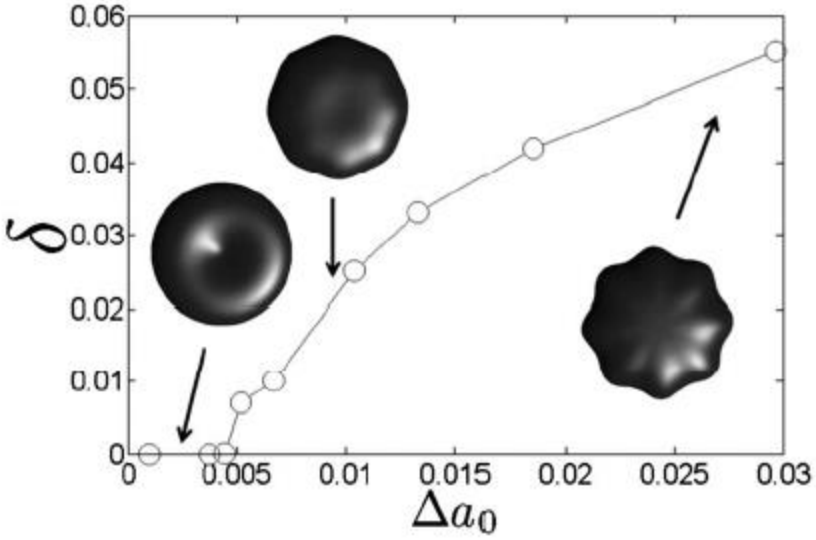

$$E_c = \frac{\kappa}{2}\int_{S_0}(\lambda_1\lambda_2 - 1)^2 \mathrm{d}S_0 + \frac{\mu}{2}\int_{S_0}\frac{(\lambda_1 - \lambda_2)^2}{2\lambda_1\lambda_2}\mathrm{d}S_0$$

$$E_b = \frac{\kappa}{2}\int_{S}(H - c_0)^2 \mathrm{d}S + \frac{\kappa_A \pi}{2AD^2}(\Delta A - \Delta A_0)^2$$

However until here we have used a „classical“ approach

Force-distance based experiments – MCF-7 cells

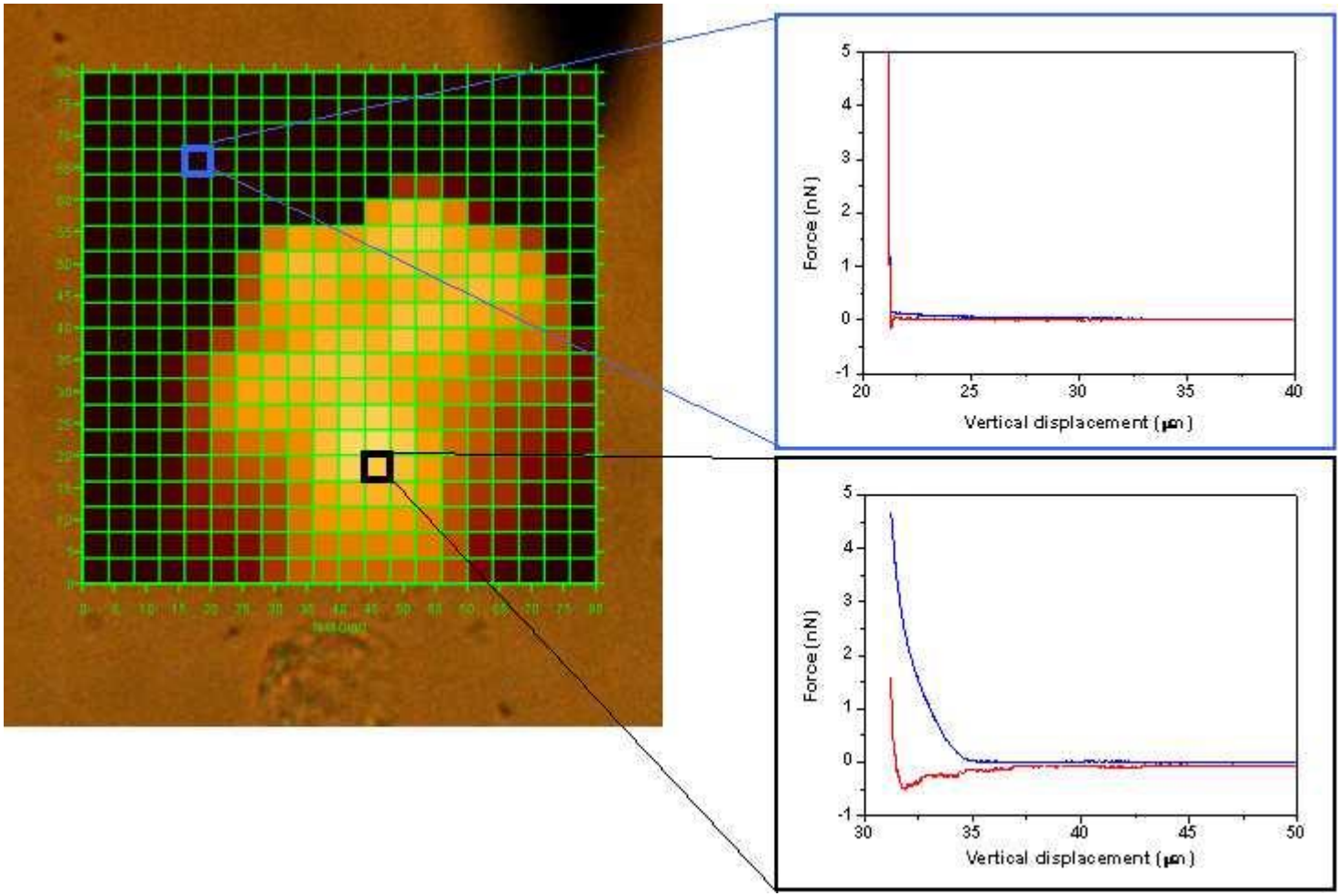

Mapping cells with the force-time based approach: relaxation

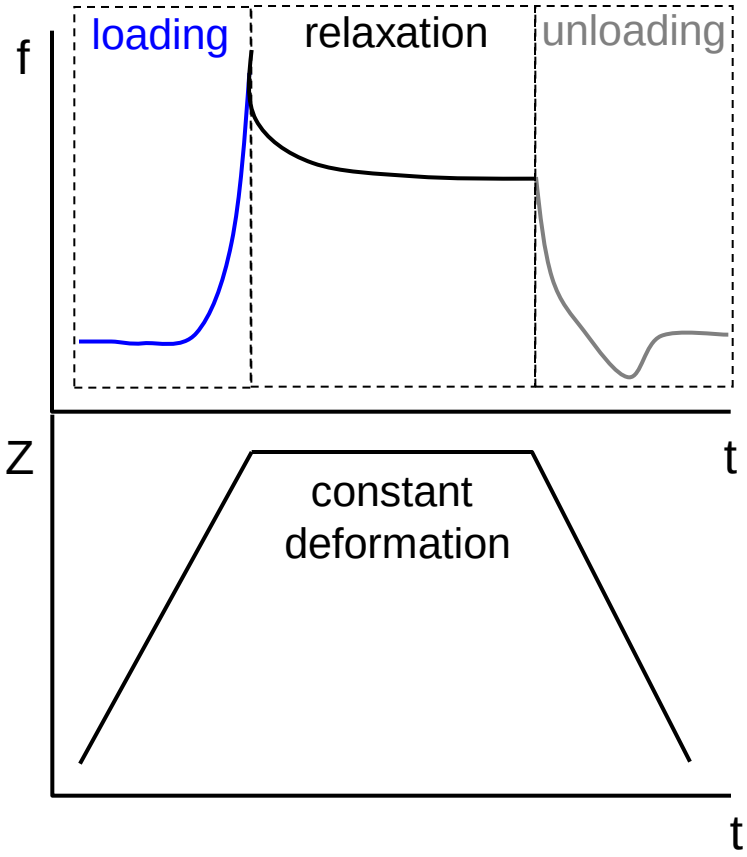

- purely elastic bodies

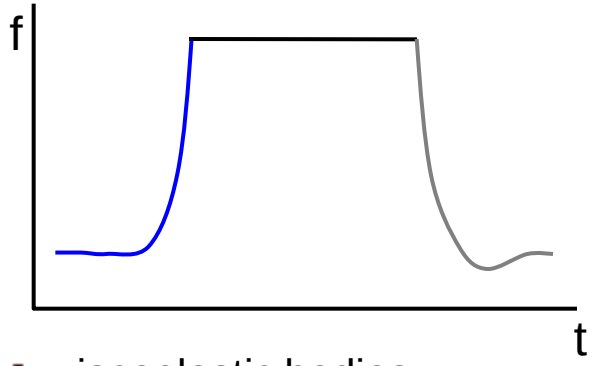

- viscoelastic bodies

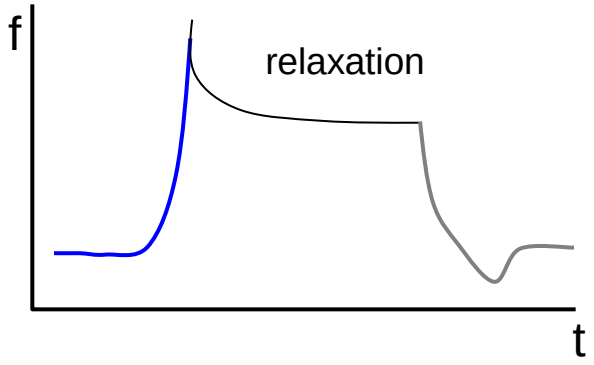

Force-time based experiments: how do MCF-7 cells relax

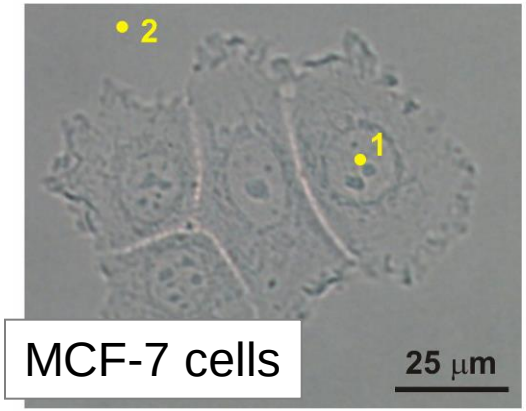

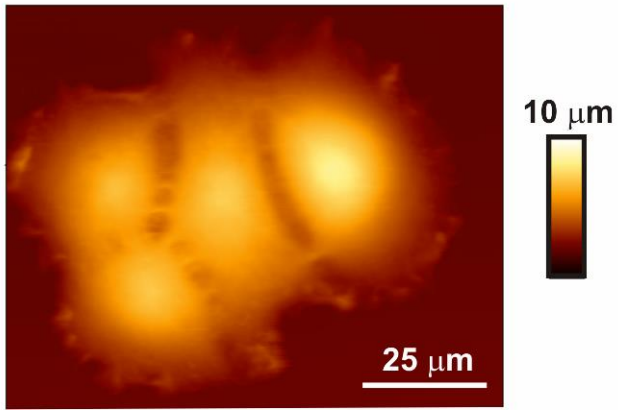

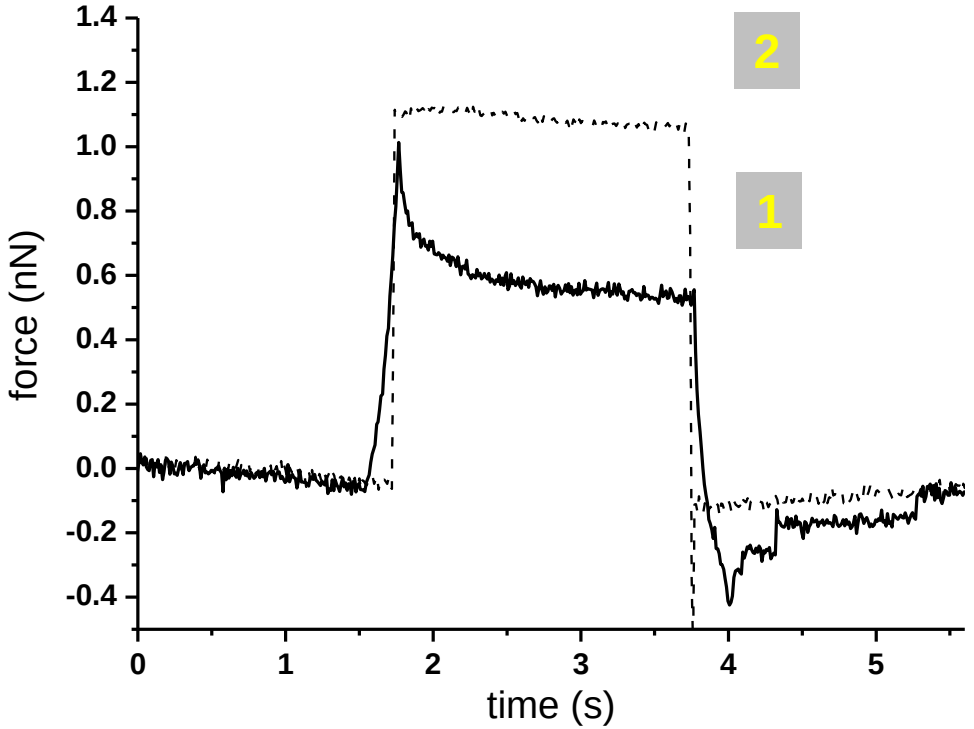

Force-time based experiments: exponential behaviour

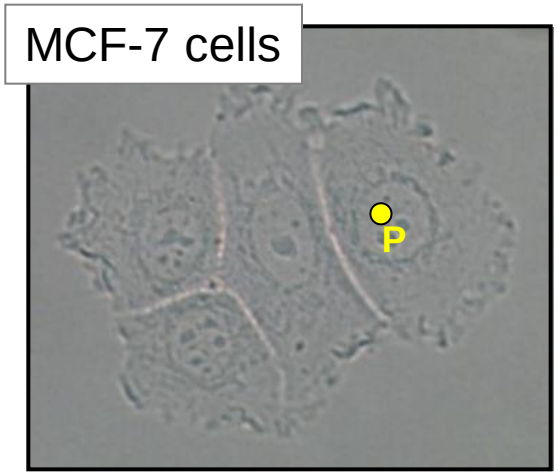

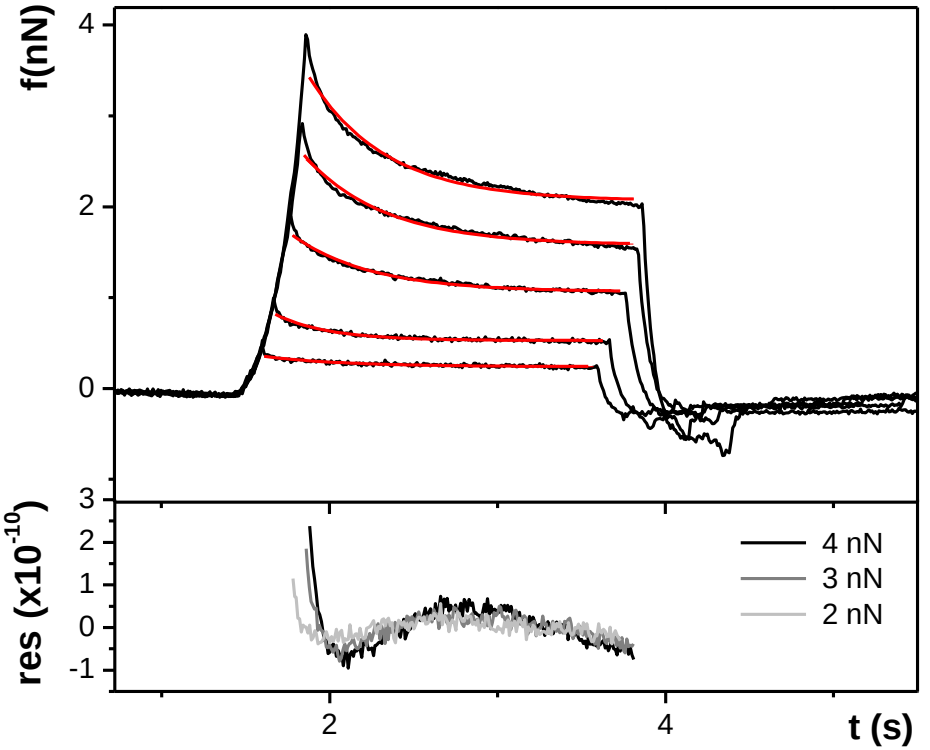

- at initial loads ≥ 1nN cell relaxation is more complex than the reported predictions on cells

- monoexponential decays are not suitable to describe cell mechanical behaviourunder these conditions

What about at looking at the parts: Force-time based experiments (bi-exponential behaviour)

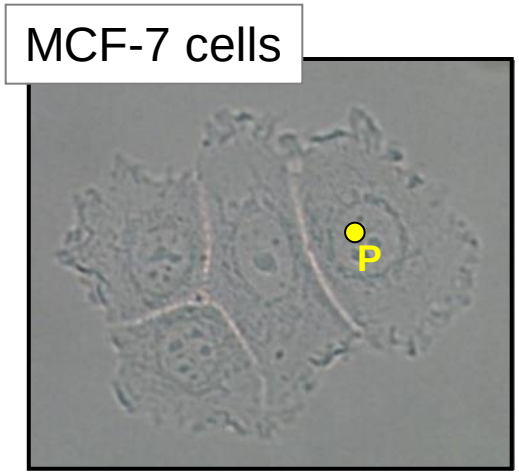

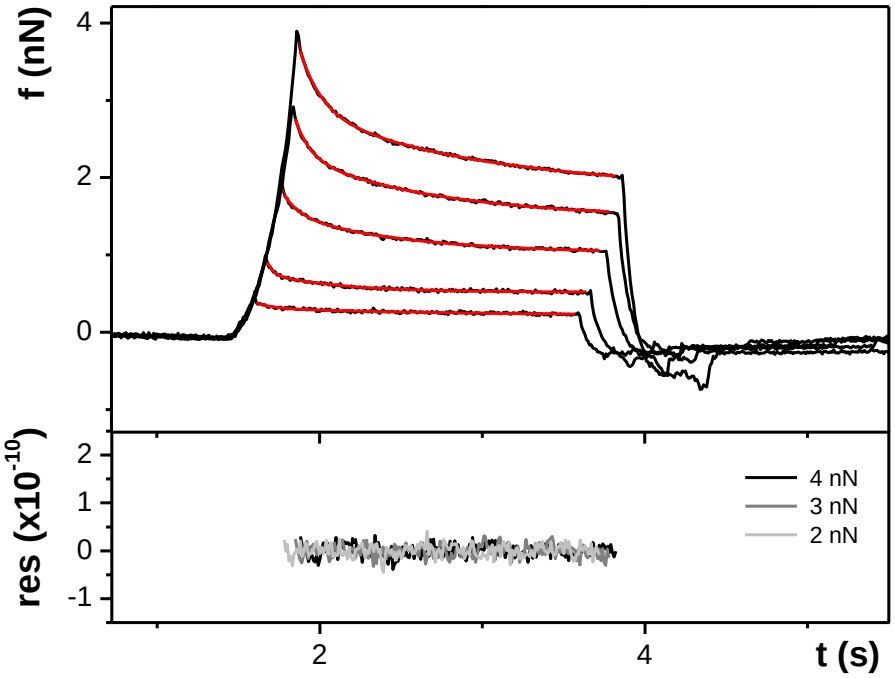

- bimodal decays: the proposed model fits reasonably well (r > 0.8)

- two simultaneously-occurring processes are detected

Stress Relaxation Microscopy (STREM): imaging decay parameters

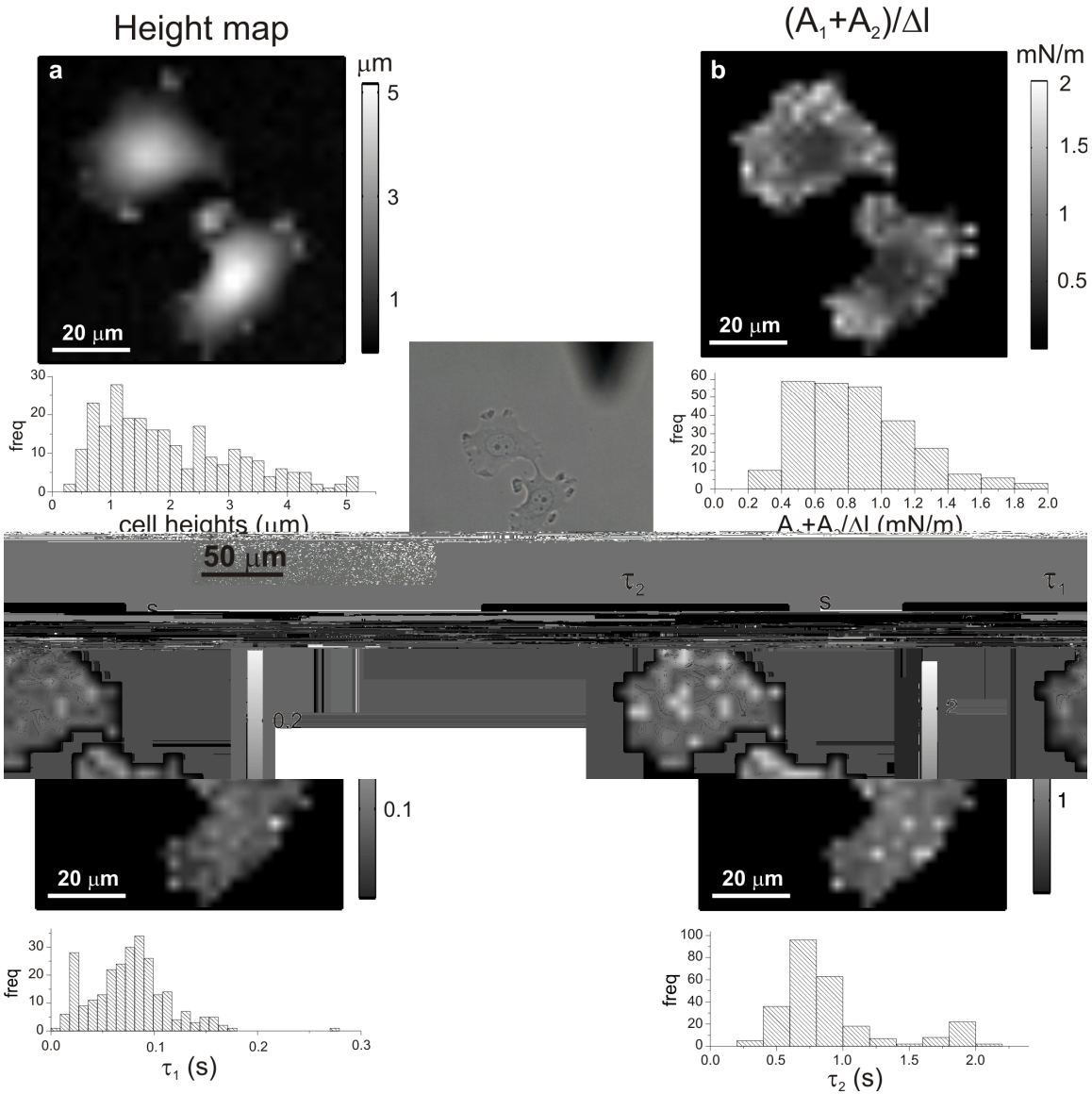

Journal of Biomechanics 43 (2010) 349

Force-time and height-time based experiments

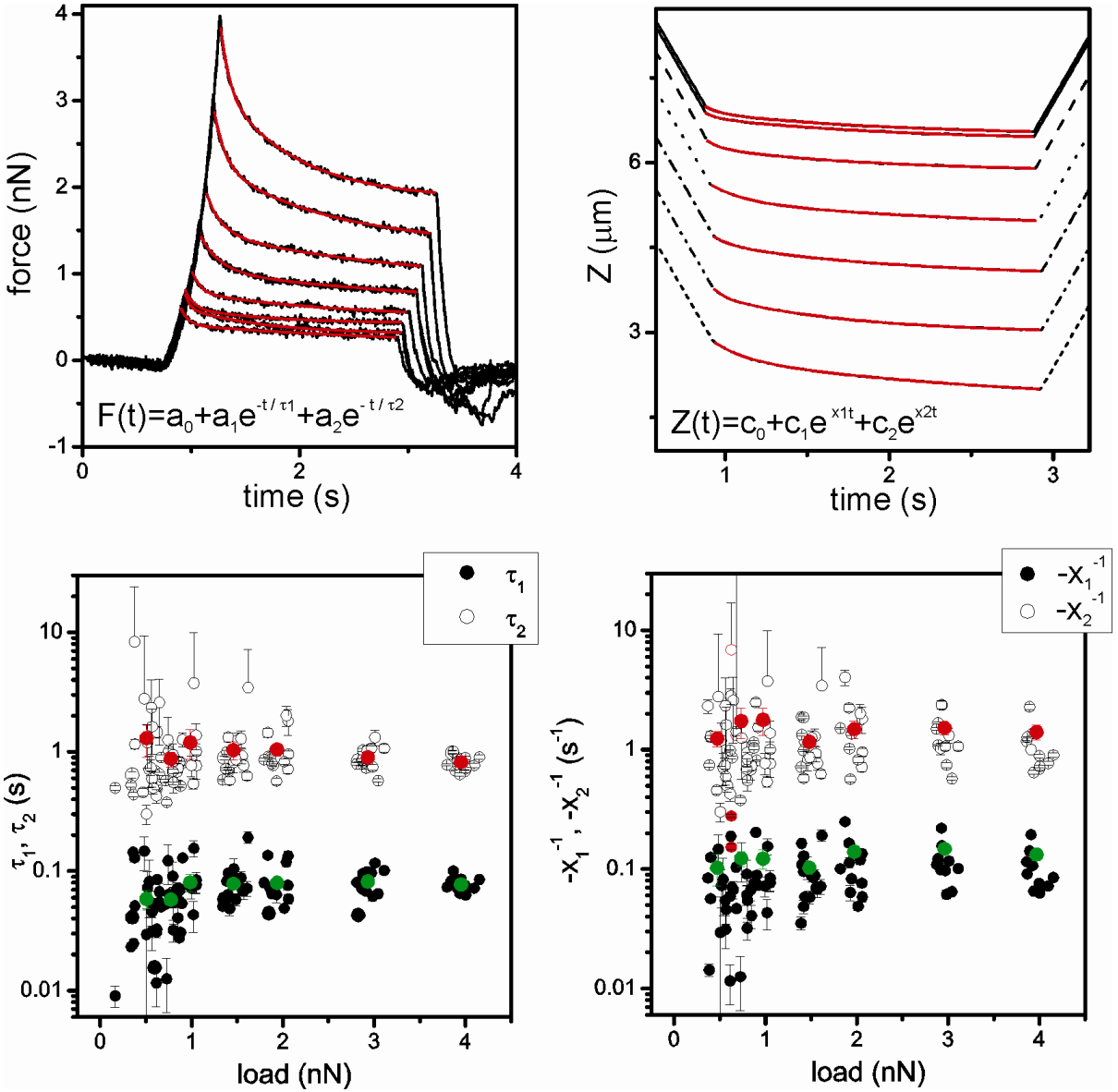

Nanotechnology 21 (2010) 445101

Stress relaxation and creep – actin-depolymerizing drug

Cytochalasin D disrupts the actin cytoskeleton
(E2 and $\eta 2$ should be more affected)

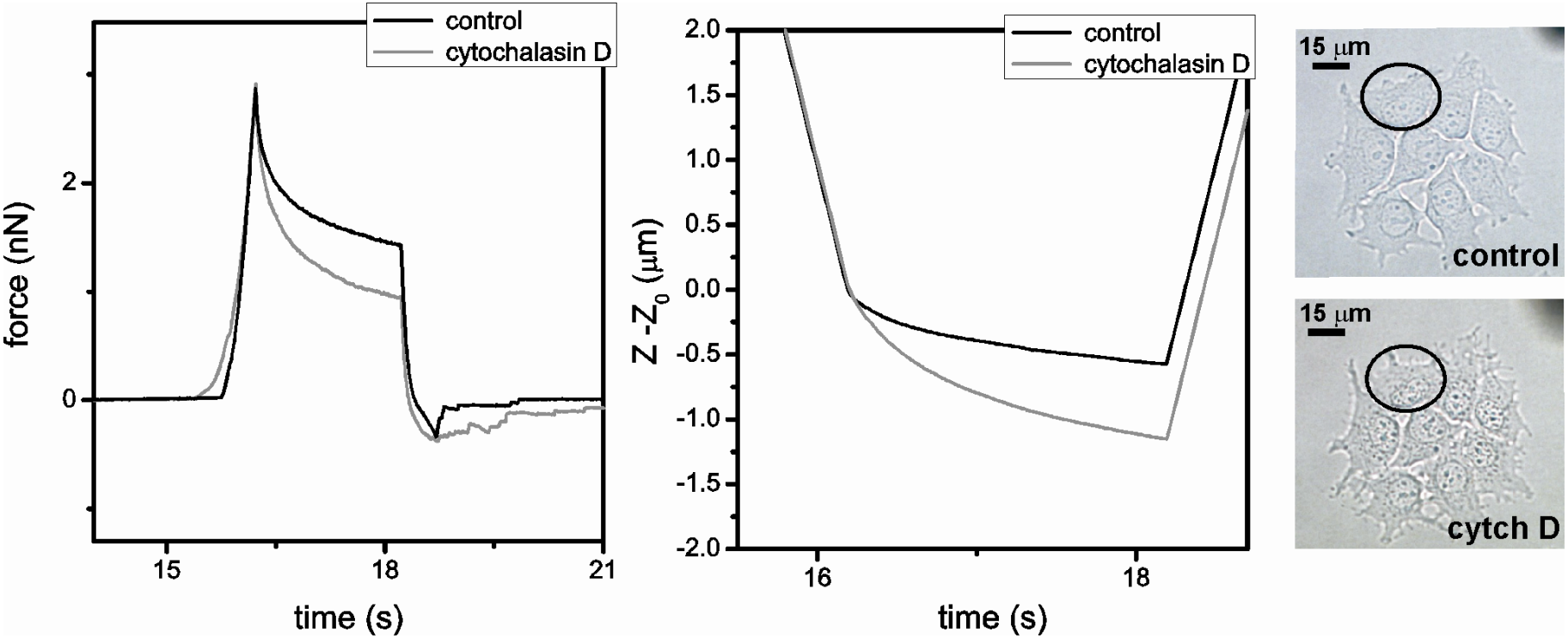

Nanotechnology 21 (2010) 445101

Actin-depolymerizing drug: results shown in another way

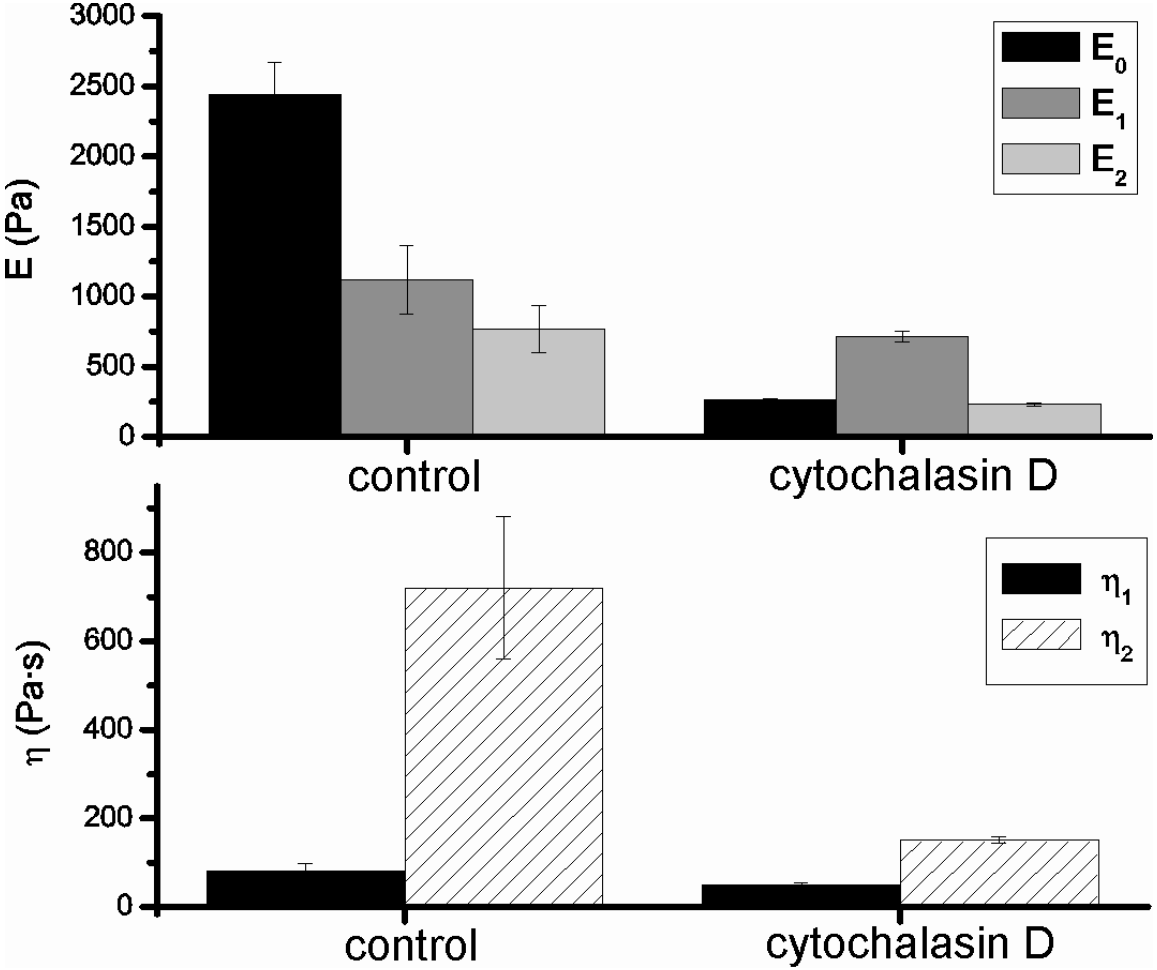

We are happy: This is nice and problematic at the same time!

Taxol stabilizes microtubules and therefore cell division

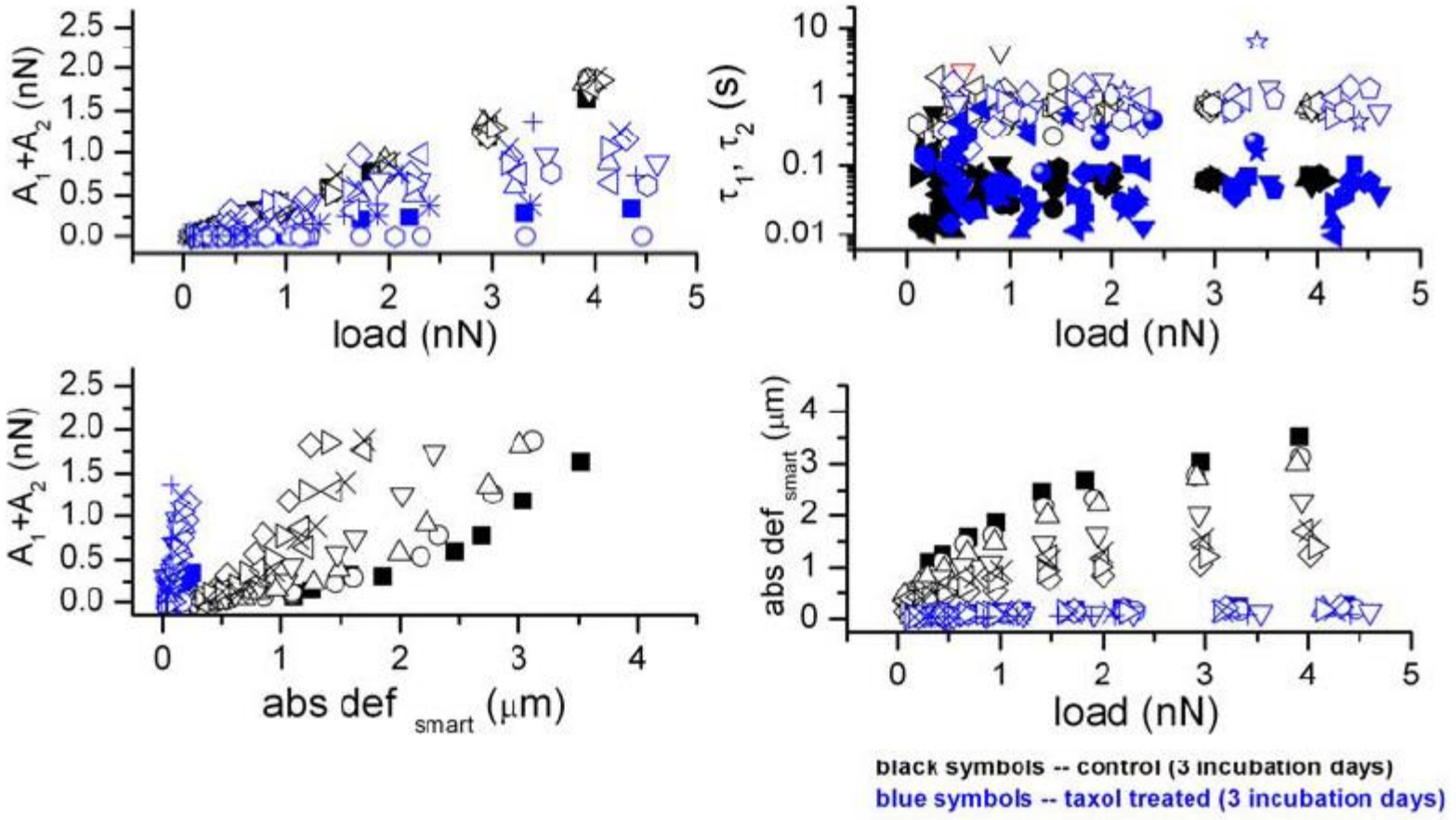

Figure 3. Stress relaxation parameters: total decay amplitud vs initial load; relaxation times vs initial load; total amplitude versus deformation; and deformation versus load

Manuscript in preparation...once we manage to understand the results ☺

There is lots of room for improvement!!!

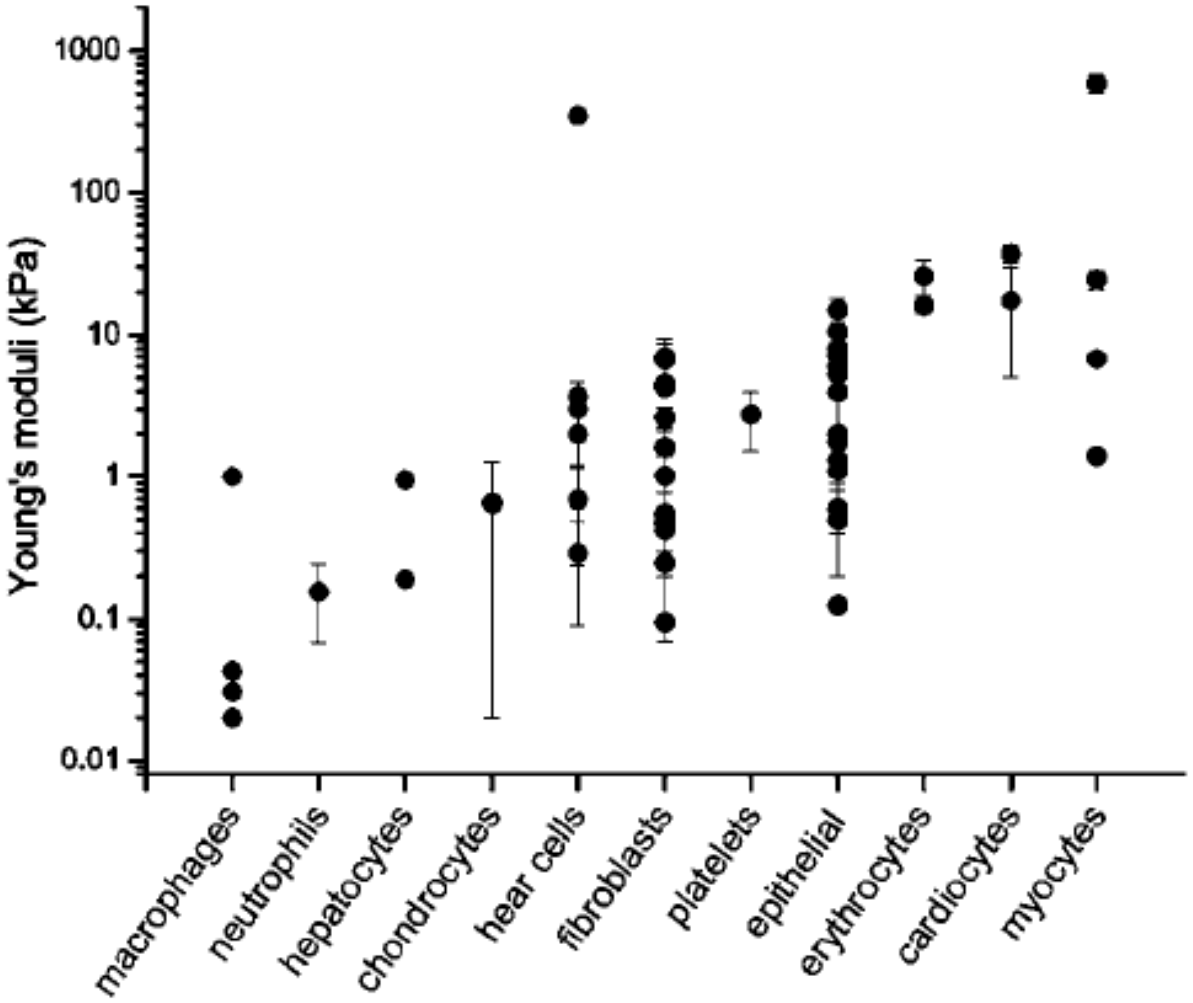

Data obtained from literature the literature of the Young's modulus of different eukaryotic cells is illustrated here.

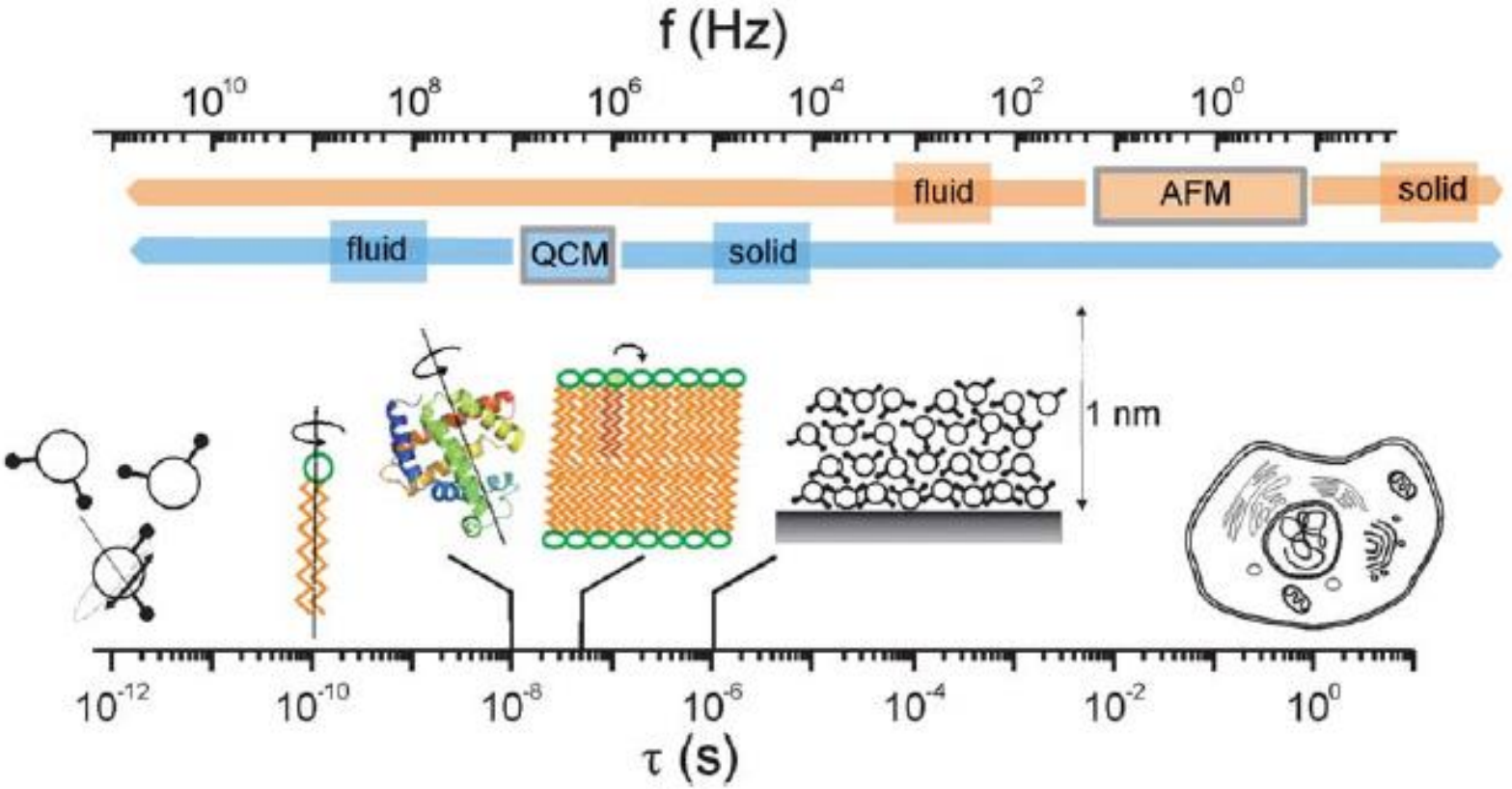

Comparison of relaxation times s for molecules and cells, and instrumental frequencies f, where f = 1/(2*pi*t). The relaxation times range from 3 ps for bulk water up to values of seconds for whole cells.

Analytical techniques that probe at high frequencies relative to 1/t will elicit solid behavior, while techniques that probe at frequencies or speeds that are slow relative to the relaxation events will elicit fluid behavior.

You can also combined force measurements with local fluorescence microscopy

Fluorescence assisted microscopy – colloidal probes

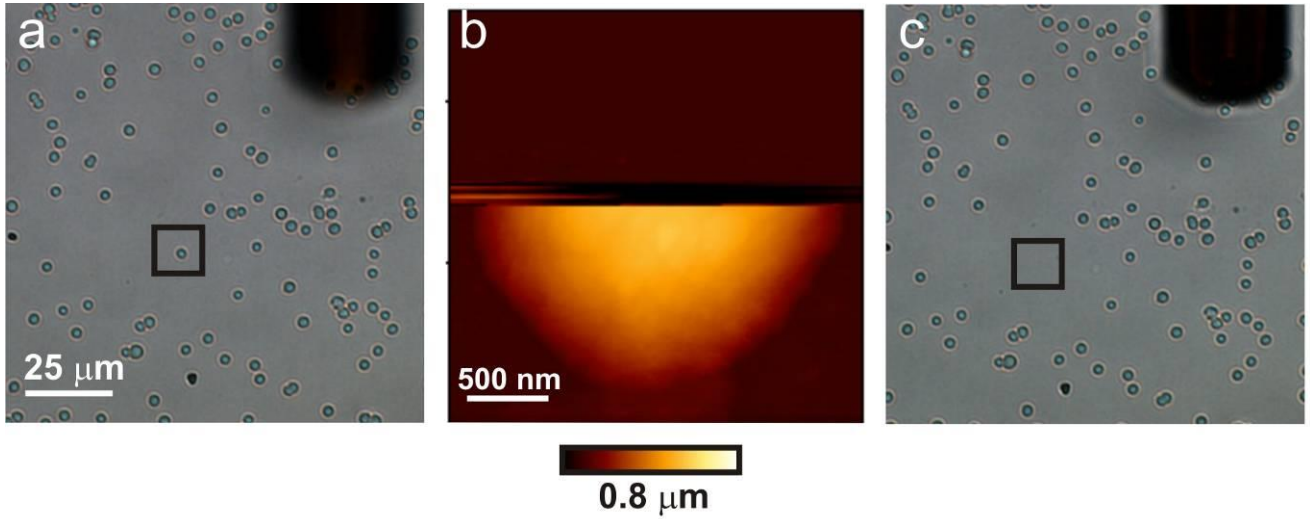

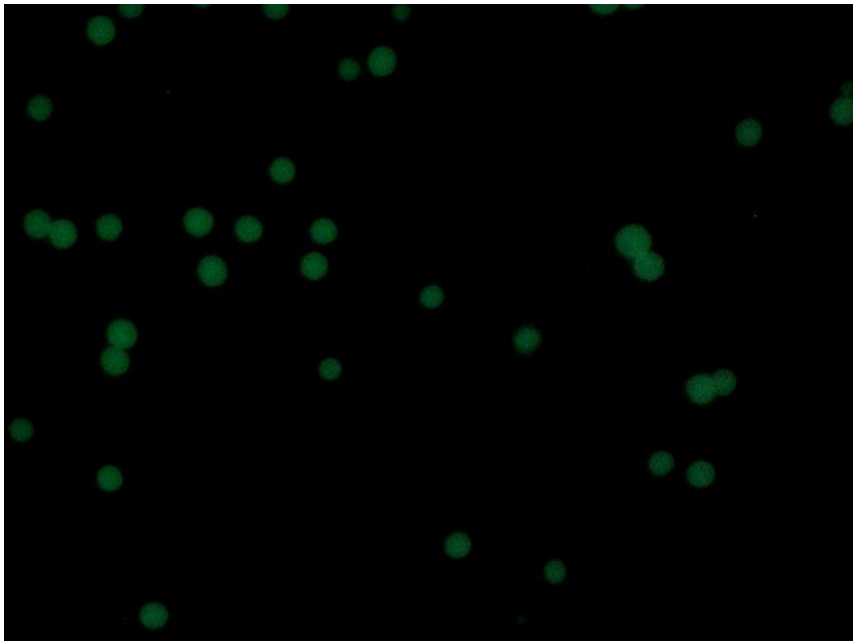

- Binding biocolloids (1-2 μm) in solution
- Particle/surface and particle/cell interaction
- Local pH determination
- Contact area evaluation?

Application to (living cells) and interfaces using colloid probes

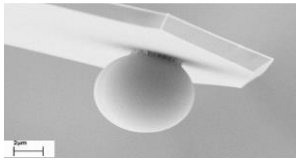

Microscopy Research and Technique 73 (2010) 746

Application: delivering carriers to single cells

Combining force-time and fluorescence microscopy we aim to:

- Monitor the incorporation of carriers through the different pathways (e.g. mechanically-induced membrane fusion, endocytosis)

- Unveil the forces & time scales involved

Technical developments going on: Raman, SPR, STED...

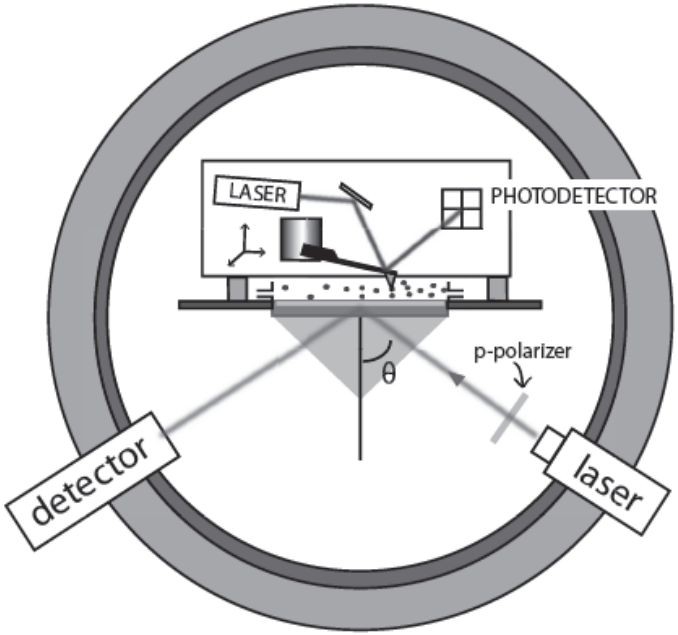

FIGURE 6.20 The combined AFM-SPR technique. An AFM head encompassing the piezo scanner, the cantilever, the aligning laser, and the photodetector can be mounted on the sample platform, whereas SPR is performed from the underside.

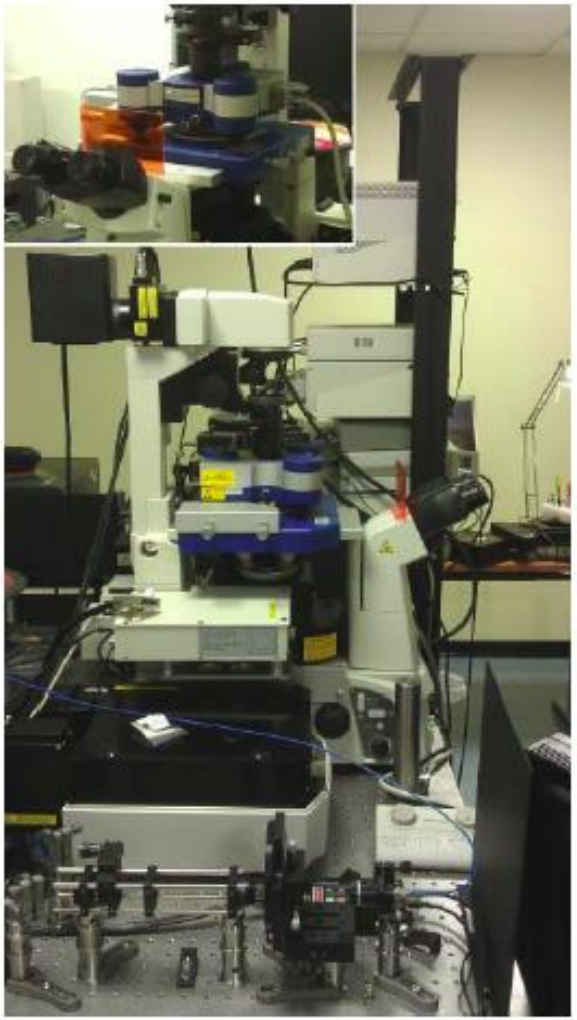

Fig. 2: Combined NanoWizard® 3 AFM and Nikon based STED system in the laboratory of Prof. Alberto Diaspro from IIT in Genua, Italy.

Moreno-Flores and Toca-Herrera, *Hybridizing Surface Probe Microscopes*, 2013, CRC Press

The message of today (reprise):

- Use the AFM if you get the change, there is a lot of room and also there is a lot of room at the top.

- It is a great technique to „visualize“ molecules, polymers, cells, etc.

- It is a great technique to measured imechanical properties of molecules, polymers, cells, etc. (also interactions between „interfaces“)

- Still theoretical questions to solve (either involving the way we measured or concerning the result interpretation).

- New technical development is always on: new measuring modes, combination with other techniques, etc.

I would like to thank the people from my group and others who showed me that cells and proteins/polymers are interesting:

Dr. Rafael Benitez - UNEX, Spain
Dr. Jaoba Iturri – BOKU, Austria
Dr. Kathryn Melzak - BOKU, Austria
Dr. Susana Moreno-Flores - BOKU, Austria
Msc. Alberto Moreno Cencerrado - BOKU, Austria
Msc. Sudarat Tharad - Mahidol Univ., Thailand
Dr. Aitziber Eleta - NanoGune, Spain
Dr. Veronica Saravia - UdR, Uruguay
Dr. Maria Vivanco - BioGUNE, Spain
Dr. Guillermo R. Lazaro - Univ. Barcelona, Spain
Prof. Aurora Hernandez - Univ. Barcelona, Spain
Prof. Ignacio Pagonabarraga - Univ. Barcelona, Spain

Prof. Helmuth Möhwald – MPI. Germany
Prof. Jane Clarke - Univ. Cambridge, UK
Dr. Robert Best - NIH, USA
Dr. Susan Fowler - Univ. Cambridge
Anette Steward - Univ. Cambridge, UK
Prof. Uwe Sleytr - BOKU, Vienna
Prof. Dietmar Pum - BOKU, Vienna

Thank you for listening
and for inviting me !!!

Force-time based experiments: the model (Zener)

Zener's model

(Riande E. et al, *Polymer viscoelasticity, Stress and strain in practice*. Marcel Dekker 2000)

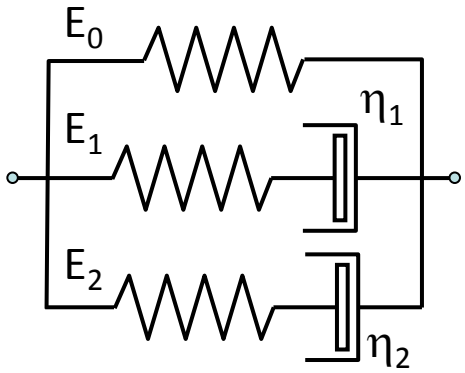

E_0, E_1 ,E_2 = compressive elastic moduli

h_1, h_2 = viscosity

$$\ddot{\sigma} + A\dot{\sigma} + B\sigma = r_2\ddot{\varepsilon} + r_1\dot{\varepsilon} + r_0\varepsilon$$

where

$$A = \frac{E_1}{\eta_1} + \frac{E_2}{\eta_2}$$

$$B = \frac{E_1 E_2}{\eta_1 \eta_2}$$

$$r_0 = \frac{E_0 E_1 E_2}{\eta_1 \eta_2}$$

$$r_1 = \frac{E_1}{\eta_1}\left(E_0 + E_2\right) + \frac{E_2}{\eta_2}\left(E_0 + E_1\right)$$

$$r_2 = E_0 + E_1 + E_2$$

For constant deformation:

$$\ddot{\sigma} + A\dot{\sigma} + B\sigma = r_0\varepsilon_0$$

the solution is

$$\sigma(t) = E_0\varepsilon_0 + A_1 e^{-t/\tau_1} + A_2 e^{-t/\tau_2}$$

$$\tau_1 = \frac{\eta_1}{E_1}, \tau_2 = \frac{\eta_2}{E_2}$$

STRESS RELAXATION

A_1, A_2, τ_1, τ_2

Force-time based experiments: the whole model (Zener)

For a constant strain/deformation

$$\ddot{\sigma} + A\dot{\sigma} + B\sigma = r_0\varepsilon_0$$

and the solution gives

$$\sigma(t) = E_0\varepsilon_0 + A_1 e^{-t/\tau_1} + A_2 e^{-t/\tau_2}$$

$$\tau_1 = \frac{\eta_1}{E_1}, \tau_2 = \frac{\eta_2}{E_2}$$

STRESS RELAXATION

A_1, A_2, τ_1, τ_2,ε_0

For a constant stress

$$r_2\ddot{\varepsilon} + r_1\dot{\varepsilon} + r_0\varepsilon = B\sigma_0$$

and the solution gives

$$\varepsilon(t) = \frac{\sigma_0}{G_1} + C_1 e^{-x_1 t} + C_2 e^{-x_2 t}$$

$$x_1 = \frac{-r_1 + \sqrt{r_1^2 - 4r_0r_2}}{2r_2}, x_2 = \frac{-r_1 - \sqrt{r_1^2 - 4r_0r_2}}{2r_2}$$

CREEP

C_1, C_2, x_1, x_2,σ_0

Elastic modulus, relaxation time and viscosity ???

Appendix. Calculation of elastic moduli and viscosities from stress relaxation and creep experiments: Zener's model

Figure 3 shows the viscoelastic model used to represent the cell's behaviour. In this model the stress can be split into the sum of three terms:

$$\sigma = \sigma_0 + \sigma_1 + \sigma_2. \tag{A.1}$$

Also we have the following equations:

$$\begin{aligned} \sigma_0 &= E_0\varepsilon \\ \dot{\varepsilon} &= \frac{\dot{\sigma}_i}{E_i} + \frac{\sigma_i}{\eta_i}, \qquad \text{for } i = 1, 2. \end{aligned} \tag{A.2}$$

Differentiating twice equation (A.2), and taking into account equation (A.1), we obtain the following three equations:

$$\sigma = E_0\varepsilon + \sigma_1 + \sigma_2 \tag{A.3}$$

$$\dot{\sigma} = \dot{\varepsilon}(E_0 + E_1 + E_2) - \frac{E_1}{\eta_1}\sigma_1 - \frac{E_2}{\eta_2}\sigma_2 \tag{A.4}$$

$$\ddot{\sigma} = \ddot{\varepsilon}(E_0 + E_1 + E_2) - \dot{\varepsilon}\left(\frac{E_1^2}{\eta_1} + \frac{E_2^2}{\eta_2}\right) + \frac{E_1^2}{\eta_1^2}\sigma_1 + \frac{E_2^2}{\eta_2^2}\sigma_2. \tag{A.5}$$

Multiplying equation (A.3) by $\frac{E_1E_2}{\eta_1\eta_2}$ and equation (A.4) by $(\frac{E_1}{\eta_1} + \frac{E_2}{\eta_2})$ and after adding these equations to (A.5) we get

$$\ddot{\sigma} + A\dot{\sigma} + B\sigma = r_2\ddot{\varepsilon} + r_1\dot{\varepsilon} + r_0\varepsilon \tag{A.6}$$

where $A = \frac{E_1}{\eta_1} + \frac{E_2}{\eta_2}$, $B = \frac{E_1E_2}{\eta_1\eta_2}$, $r_0 = \frac{E_0E_1E_2}{\eta_1\eta_2}$, $r_1 = \frac{E_1E_2}{\eta_1\eta_2}(E_0 + E_2) + \frac{E_1E_2}{\eta_1\eta_2}(E_0 + E_1)$ and $r_2 = E_0 + E_1 + E_2$.

A.1. Experiments at constant strain: stress relaxation

Let us consider the particular case of a constant strain $\varepsilon(t) = \varepsilon_0$. Then equation (A.6) reduces to

$$\ddot{\sigma} + A\dot{\sigma} + B\sigma = r_0\varepsilon_0. \tag{A.7}$$

The general solution to equation (A.7) has the form $\sigma(t) = \sigma_p(t) + \sigma_0(t)$, where $\sigma_0(t)$ is the general solution of the homogeneous equation $\ddot{\sigma} + A\dot{\sigma} + B\sigma = 0$ and $\sigma_p(t)$ is a particular solution of (A.7). Since the right-hand side of equation (A.7) is constant we may find a constant particular solution $\sigma_p(t) = E_0\varepsilon_0$. On the other hand, the general solution of the homogeneous equation takes the form $\sigma_0(t) = A_1e^{-t/\tau_1} + A_2e^{-t/\tau_2}$, with $\tau_i = \frac{\eta_i}{E_i}$ for $i = 1, 2$. Therefore the general solution of equation (A.7) is

$$\sigma(t) = E_0\varepsilon_0 + A_1e^{-t/\tau_1} + A_2e^{-t/\tau_2}. \tag{A.8}$$

A.2. Experiments at constant height: creep

Considering now a constant stress $\sigma(t) = \sigma_0$ equation (A.6) takes the form

$$r_2\ddot{\varepsilon} + r_1\dot{\varepsilon} + r_0\varepsilon = B\sigma_0. \tag{A.9}$$

The particular solution to this equation is given by the constant function $\varepsilon_p(t) = \frac{B\sigma_0}{r_0} = \frac{\sigma_0}{E_0}$. The general solution to the homogeneous equation $r_2\ddot{\varepsilon} + r_1\dot{\varepsilon} + r_0\varepsilon = 0$ is given by $\varepsilon_0(t) = C_1e^{x_1t} + C_2e^{x_2t}$; x_1 and x_2 are the roots of the characteristic polynomial $r_2x^2 + r_1x + r_2$ which are given by

$$x_1 = \frac{-r_1 + \sqrt{r_1^2 - 4r_0r_2}}{2r_2}, \qquad x_2 = \frac{-r_1 - \sqrt{r_1^2 - 4r_0r_2}}{2r_2}. \tag{A.10}$$

Both are real and negative, because $r_1^2 - 4r_0r_1 = (\frac{E_1}{\eta_1}(E_0 + E_2) - \frac{E_2}{\eta_2}(E_0 + E_1))^2 + \frac{4E_0^2E_1^2}{\eta_1\eta_2} > 0$. Thus the general solution to equation (A.5) is

$$\varepsilon(t) = \frac{\sigma_0}{E_0} + C_1e^{x_1t} + C_2e^{x_2t}. \tag{A.11}$$

A.3. Obtaining parameters

We assume we have experimentally obtained two signals that follow Zener's model. Then we have

$$\sigma(t) = A_0 + A_1e^{-t/\tau_1} + A_2e^{-t/\tau_2} \tag{A.12}$$

$$\varepsilon(t) = C_0 + C_1e^{x_1t} + C_2e^{x_2t}. \tag{A.13}$$

To obtain the coefficients E_0, E_1, E_2, η_1, η_2 and η_3 from the experimental coefficients A_0, τ_1, τ_2, C_0, x_1 and x_2, we assume we know σ_0 and ε_0. E_0 is thus easily obtained as

$$E_0 = \frac{A_0}{\varepsilon_0}. \tag{A.14}$$

We can in turn get the value of r_0 from its definition and E_0, $r_0 = \frac{E_0E_1E_2}{\eta_1\eta_2} = \frac{E_0}{\tau_1\tau_2}$. Knowing r_0, we can obtain r_1 and r_2 in terms of x_1, x_2 and r_0 by multiplying the expressions of x_1 and x_2, $x_1x_2 = \frac{r_1^2 - (\sqrt{r_1^2 - 4r_0r_2})^2}{4r_2^2} = \frac{r_0r_2}{r_2^2} = \frac{r_0}{r_2}$. We thus obtain r_2 as

$$r_2 = \frac{r_0}{x_1x_2} \tag{A.15}$$

and r_1 as

$$r_1 = -r_2x_1 - \frac{r_0}{x_1} = -r_0\left(\frac{1}{x_1} + \frac{1}{x_2}\right). \tag{A.16}$$

We can then rewrite the expressions of r_2 and r_1 in terms of E_0, τ_1, τ_2, r_1 and r_2 as follows:

$$\begin{aligned} E_1 + E_2 &= r_2 - E_0 \\ \frac{E_1}{\tau_2} + \frac{E_2}{\tau_1} &= r_1 - E_0\left(\frac{1}{\tau_1} + \frac{1}{\tau_2}\right). \end{aligned} \tag{A.17}$$

Equations (A.17) are a system of two linear equations with two unknowns (E_1 and E_2). The solution gives

$$\begin{aligned} E_1 &= r_2 - \left[E_0 + \frac{1}{(\frac{1}{\tau_1} - \frac{1}{\tau_2})}\left(r_1 - \frac{r_2}{\tau_2} - \frac{E_0}{\tau_1}\right)\right] \\ E_2 &= \frac{1}{(\frac{1}{\tau_1} - \frac{1}{\tau_2})}\left(r_1 - \frac{r_2}{\tau_2} - \frac{E_0}{\tau_1}\right) \end{aligned} \tag{A.18}$$

which turns to

$$E_1 = \frac{A_0}{\varepsilon_0}\left[\frac{1}{(1 - \frac{\tau_1}{\tau_2})}\left(1 + \frac{1}{x_1\tau_1} + \frac{1}{x_2\tau_2} + \frac{1}{x_1x_2\tau_2^2}\right) + \frac{1}{x_1x_2\tau_1\tau_2} - 1\right] \tag{A.19}$$

$$E_2 = \frac{A_0}{\varepsilon_0(1 - \frac{\tau_1}{\tau_2})}\left(-\frac{1}{x_1x_2\tau_2^2} - \frac{1}{x_1\tau_2} - \frac{1}{x_2\tau_2} - 1\right)$$

as a function of the experimental parameters. Once E_1 and E_2 are known, it is possible to calculate the viscosities η_1 and η_2 by substitution into their respective expressions:

$$\eta_1 = E_1\tau_1 = \frac{A_0\tau_1}{\varepsilon_0}\left[\frac{1}{(1 - \frac{\tau_1}{\tau_2})}\left(1 + \frac{1}{x_1\tau_1} + \frac{1}{x_2\tau_2} + \frac{1}{x_1x_2\tau_2^2}\right) + \frac{1}{x_1x_2\tau_1\tau_2} - 1\right] \tag{A.20}$$

$$\eta_2 = E_2\tau_2 = \frac{A_0\tau_2}{\varepsilon_0(1 - \frac{\tau_1}{\tau_2})}\left(-\frac{1}{x_1x_2\tau_2^2} - \frac{1}{x_1\tau_2} - \frac{1}{x_2\tau_2} - 1\right).$$

Table 1
Selected published values of diffusion coefficient obtained by FCS.

Model[a]	Composition[b]	Tracer[b]	T [°C][c]	Phase[d]	FCS[e]	D [$\mu m^2 s^{-1}$]	Ref.
GUV	DLPC	Dil-C_{20}	23		sp	4.4 ± 0.9	[86]
GUV	DLPC	Dil-C_{20}	25		sp	3.0 ± 0.6	[218]
GUV	DLPC	Dil-C_{18}			sp	6.5 ± 0.5	[216]
GUV	DOPC/SM/Chol 2/2/1	DiO	20	L_α^d	Z	6.1 ± 0.5	
				L_α^o		2.5 ± 0.2	[222]
GUV	DOPC/DSPC 1/1	Dil-C_{18}		L_α^d	sp	6.5 ± 0.4	[219]
GUV	DOPC/DSPC/Chol 5/5/2	Dil-C_{18}		L_α^d	sp	5.1 ± 0.4	
				L_α^o		0.13 ± 0.02	[219]
GUV	DOPC/DSPC/Chol 1/1/1	Dil-C_{18}			sp	1.4 ± 0.1	[219]
GUV	DLPC/DPPC 3/2	Dil-C_{20}	25	L_α^d	sp	5 ± 1	
				L_β		0.020 ± 0.004	[218]
GUV	POPC	Dil-C_{18}			RICS	7 ± 3	[170]
SLB m	DOPC	Rh DHPE			Z	4.2 ± 0.4	[129]
SLB m	DOPC/Chol 7/3	Rh DHPE			Z	1.1 ± 0.2	[129]
SLB m	DOPC	Rh DHPE			Z	4.0 ± 0.5	[129]
SLB q	DLPC	Rh DMPE	23		sp	2.6 ± 0.2	[203]
SLB m	DOPC/SM/Chol	BodChol		L_α^d	2-fs	3.4 ± 0.3	
				L_α^o		0.11 ± 0.02	[153]
SLB m	DOPC/SM/Chol	DiD		L_α^d	2-fs	1.5 ± 0.1	
				L_α^o		0.16 ± 0.04	[153]
FPM	DPhPS	Rh DOPE			sp	8.1 ± 0.4	[33]

[a] Abbreviations: m, mica; g, glass; q, quartz; FPM, free-standing planar membrane, see the reference for details.
[b] Abbreviations: DLPC, dilauroyl-phosphocholine; DOPC, dioleoyl-phosphocholine; DSPC, distearoyl-phosphocholine; DPPC, dipalmitoyl-phosphocholine; DPhPS, diphytanoyl-phosphoserine; SM, sphingomyelin; Chol, Cholesterol; DOPE, dioleoyl-phosphoethanolamine; DHPE, dihexadecanoyl-phosphoethanolamine; Rh, Rhodamine; Bod, Bodipy.
[c] Ambient if not specified otherwise.
[d] Phase specified if more phases coexisted in the sample.
[e] Abbreviations: sp, single-point FCS; Z, Z-scan FCS; 2-fs, 2-focus scanning FCS.

A nice alternative to the „standard“ model ...

Macromolecules

Article

pubs.acs.org/Macromolecules

Indentation of Highly Charged PSPM Brushes Measured by Force Spectroscopy: Application of a Compressible Fluid Model

José Luis Cuellar,[†] Irantzu Llarena,[‡] Sergio Enrique Moya,[*,‡,§] and Edwin Donath[†]

[†]Institute of Biophysics and Medical Physics, Faculty of Medicine, University of Leipzig, Leipzig, Germany

[‡]CIC biomaGUNE, Paseo Miramón 182 C, 20009 San Sebastian, Spain

[§]Department of Polymer Science and Engineering, Zhejiang University, Hangzhou 310027, China

Supporting Information

ABSTRACT: Highly charged dense poly(sulfopropyl methacrylate) polyelectrolyte brushes were indented with an atomic force microscopy (AFM) tip as well as with an 8 μm silica colloidal probe at different ionic strengths ranging from Millipore water to 1 M NaCl. The force response during indentation was fitted to a phenomenological equation analogous to the equation of state of a compressible fluid. In this way, internal energy and brush thickness were obtained as a function of ionic strength. Long-range forces decayed exponentially with distance. The characteristic decay lengths were much larger than the Debye screening lengths at the respective ionic strengths. It was therefore concluded that long-range repulsion was due to compression of a loose corona of polymers in front of the dense part of the brush. The size of the indentor determines which region of the brush can be explored by AFM. The tip probes the denser parts of the brush, while with the colloidal probe the corona of the brush can be investigated. The obtained fits of the experimentally measured force distance curves were used as regularization tools for obtaining the brush swelling pressure or “force per unit area” as a function of brush compression. The swelling pressure as a function of brush thickness, h, followed over a wide range a power law close to $\sim h^{-2}$. This approach allowed deriving fundamental brush parameters on a thermodynamical basis like the compressibility as a function of thickness.

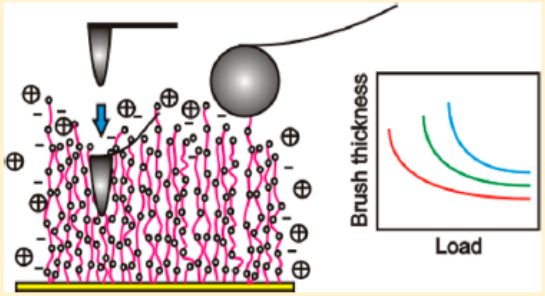

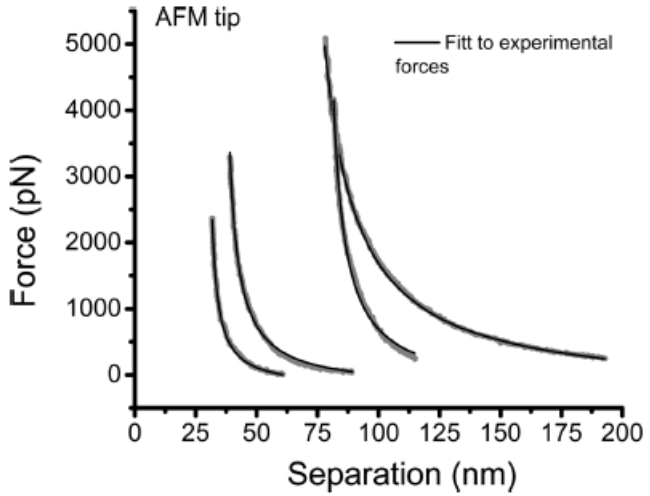

Figure 4. Forces versus distance curves measured with the AFM tip at different salt concentrations. From left to right the salt concentration was 1000, 100, and 10 mM NaCl and Millipore water. The solid black lines represent the least-squares fits of the experimental data to eq 2.

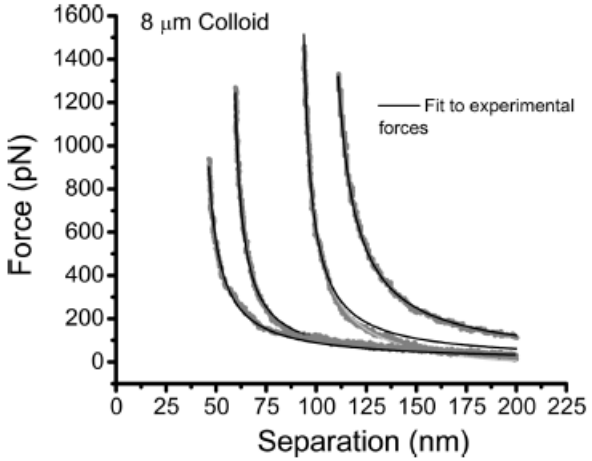

Figure 5. Forces versus distance curves measured with the colloidal probe at different salt concentrations. From left to right, the salt concentration was 1000, 100, and 10 mM NaCl and Millipore water. The solid black lines represent the least-squares fits of the experimental data to eq 4. The light gray solid line represents the best fit for the case of 10 mM NaCl without taking into account the parameter.

The model is based on an equation similar equation of state of a compressible fluid.

The model provides the brush thickness, the internal energy, and of the compressibility (as a function of ionic strength, e.g molecular arrangement of the polymer chains) as the ionic strength changes. as applied to nanotechnology.

Alternative when the measured force indentation relationships were inconsistent with linear elastic theories.

HYBRIDIZING SURFACE PROBE MICROSCOPIES

Toward a Full Description of the Meso- and Nanoworlds

SUSANA MORENO-FLORES
JOSE L. TOCA-HERRERA

CRC Press
Taylor & Francis Group

Outlook (III)…going on

-echinocytes were formed by storage of RBCs in plasma, followed by rinsing with phosphate buffered saline

-application of 6 nN or more causes a shape change

-application of 3 nN or less typically does not

- same effect is observed when the ATP-dependent translocases are inhibited (with vanadate)

-the smoother cell shapes are stable for periods of several hours

Red blood cells and their shapes:

Healthy red blood cells in vivo have a biconcave disc shape.

photograph (light microscope)

The disc shape is associated with minimisation of the bending energy that arises because the lipid bilayer is asymmetric. The relative areas of

Key idea (?)

But proteins don't just fold one time and that's it.

Mechanical unfolding of proteins may be important in translocation and degradation and in mechanically active proteins

For some proteins resisting unfolding may be important

Combining force-distance and force-time approaches. Designing own tips to have a clear surface contact interaction

OPEN ACCESS Freely available online

PLoS one

Integrin-Specific Mechanoresponses to Compression and Extension Probed by Cylindrical Flat-Ended AFM Tips in Lung Cells

Irene Acerbi[1,2,3], Tomás Luque[1,3], Alícia Giménez[1], Marta Puig[1,4], Noemi Reguart[5], Ramon Farré[1,4,5], Daniel Navajas[1,3,5], Jordi Alcaraz[1,5]*

1 Unitat de Biofísica i Bioenginyeria, Facultat de Medicina, Universitat de Barcelona, Barcelona, Spain, **2** Laboratorio di Tecnologie Biomediche, Dipartimento di Bioingegneria, Politecnico di Milano, Milano, Italy, **3** Institut de Bioenginyeria de Catalunya (IBEC), Barcelona, Spain, **4** Institut d'Investigacions Biomèdiques August Pi i Sunyer (IDIBAPS), Barcelona, Spain, **5** CIBER de Enfermedades Respiratorias (CIBERES), Bunyola, Spain

Abstract

Cells from lung and other tissues are subjected to forces of opposing directions that are largely transmitted through integrin-mediated adhesions. How cells respond to force bidirectionality remains ill defined. To address this question, we nanofabricated flat-ended cylindrical Atomic Force Microscopy (AFM) tips with ~1 μm^2 cross-section area. Tips were uncoated or coated with either integrin-specific (RGD) or non-specific (RGE/BSA) molecules, brought into contact with lung epithelial cells or fibroblasts for 30 s to form focal adhesion precursors, and used to probe cell resistance to deformation in compression and extension. We found that cell resistance to compression was globally higher than to extension regardless of the tip coating. In contrast, both tip-cell adhesion strength and resistance to compression and extension were the highest when probed at integrin-specific adhesions. These integrin-specific mechanoresponses required an intact actin cytoskeleton, and were dependent on tyrosine phosphatases and Ca^{2+} signaling. Cell asymmetric mechanoresponse to compression and extension remained after 5 minutes of tip-cell adhesion, revealing that asymmetric resistance to force directionality is an intrinsic property of lung cells, as in most soft tissues. Our findings provide new insights on how lung cells probe the mechanochemical properties of the microenvironment, an important process for migration, repair and tissue homeostasis.